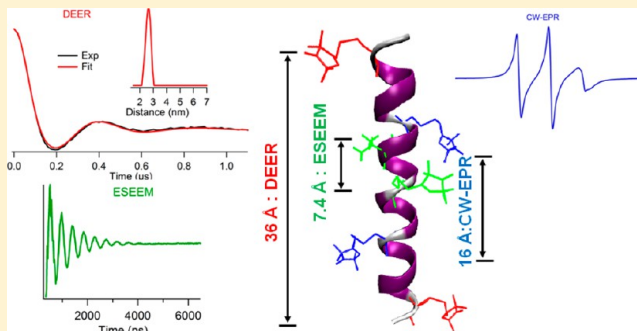# Use of Electron Paramagnetic Resonance To Solve Biochemical Problems

Indra D. Sahu, Robert M. McCarrick, and Gary A. Lorigan*

Department of Chemistry and Biochemistry, Miami University, Oxford, Ohio 45056, United States

ABSTRACT: Electron paramagnetic resonance (EPR) spectroscopy is a very powerful biophysical tool that can provide valuable structural and dynamic information about a wide variety of biological systems. The intent of this review is to provide a general overview for biochemists and biological researchers of the most commonly used EPR methods and how these techniques can be used to answer important biological questions. The topics discussed could easily fill one or more textbooks; thus, we present a brief background on several important biological EPR techniques and an overview of several interesting studies that have successfully used EPR to solve pertinent biological problems. The review consists of the following sections: an introduction to EPR techniques, spin-labeling methods, and studies of naturally occurring organic radicals and EPR active transition metal systems that are presented as a series of case studies in which EPR spectroscopy has been used to greatly further our understanding of several important biological systems.

INTRODUCTION TO ELECTRON PARAMAGNETIC RESONANCE-BASED METHODS

Electron Paramagnetic Resonance (EPR) Spectroscopy. EPR spectroscopy requires the presence of an unpaired electron spin. Historically, this has limited the scope of biological systems that could be studied using EPR to those containing organic-based radicals or EPR active transition metals. The advent of spin-labeling methods has expanded the technique to include proteins and nucleotides into which an unpaired electron spin can be introduced.[1,2] The simplest EPR active system consists of a single unpaired electron spin residing in a molecular orbital. The electron can exist in one of two M_s quantum states, $+^1/_2$ and $-^1/_2$. In the absence of a magnetic field, these two states are degenerate and have the same energy. However, when a magnetic field is applied, the energy of the $-^1/_2$ state decreases and the energy of the $+^1/_2$ state increases as a function of the strength of the magnetic field as seen in Figure 1.[3]

The energy separation between the two spin states is $g\beta_e B_0$, where g is a proportionality factor that can considered to be similar to a chemical shift parameter in nuclear magnetic resonance (NMR), β_e is the electron Bohr magneton, and B_0 is the strength of the static magnetic field. Contrary to NMR studies, in which continuous wave (CW) experiments have been replaced with pulsed methods, CW EPR is the most frequently used spectroscopic technique. In a typical CW-EPR experiment, a constant microwave frequency is applied and the B_0 magnetic field is swept with spin-flip transitions occurring when the energy separation between the two electron spin states matches the constant microwave energy. In addition to the sweep of B_0, the field is typically modulated to enhance the signal-to-noise ratio of the spectra. This gives rise to the

$$\beta_e \equiv \frac{|e|\hbar}{2\,m_e} = 9.27400949 \times 10^{-24}\frac{J}{T}$$
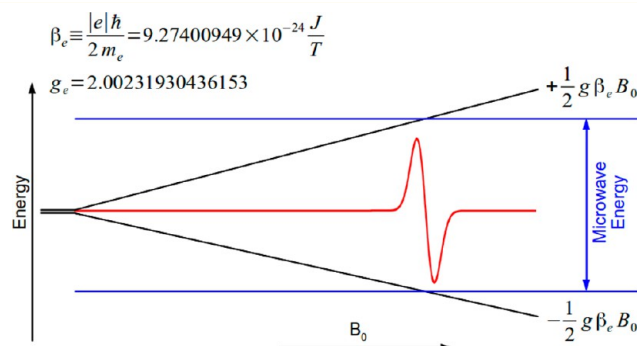
$$g_e = 2.00231930436153$$

Figure 1. EPR transitions occur when the energy contained in the microwave photons matches the splitting between two electron spin states. In the simplest system, this splitting as a function of the magnetic field is $g\beta_e B_0$.

derivative line shape typically observed in most EPR spectra, as it is essentially the slope of the signal that is being measured as the bulk magnetic field is swept and not the signal itself. As depicted in Figure 1, the derivative-shaped signal occurs when the separation in energy between the two spin states matches the applied microwave radiation.

The magnetic field at which this signal appears depends on the g value, which dictates the slope at which the energy levels for the two spin states change as a function of the magnetic field. A free electron in a vacuum has a g value (g_e) of 2.00231930436153 (uncertainty of 0.00000000000053), which

is one of the most precisely known values in physics.[3] Shifts from this value occur because of spin orbit coupling within the molecule. In most biological systems, the g value is anisotropic with an orientation dependence meaning that the effective g value is different depending on the orientation of the molecule with respect to the applied magnetic field.

The EPR spectrum is also dependent on interactions between the electron spin and any NMR active nuclei in the vicinity. This interaction is termed the hyperfine interaction (A) and depends on the amount of electron spin density on the nucleus, the distance between the electron spin and the nucleus, and the angle between the two with respect to the magnetic field. Like the g value, this is also often orientation-dependent. Other parameters that can be extracted from an EPR spectrum are electron–electron couplings between two sets of spins that can provide valuable distance information between biological systems and zero-field splittings in higher-spin systems. The information that can be obtained through the extraction of these parameters will be discussed in the following sections on spin-labeled and naturally occurring EPR active systems.

Electron Nuclear Double Resonance (ENDOR) Spectroscopy, Electron Spin Echo Envelope Modulation (ESEEM), and Hyperfine Sublevel Correlation (HYSCORE) Spectroscopic Techniques. In ENDOR, ESEEM, and HYSCORE spectroscopies, the electron spin is essentially used as a detector to probe nuclei that are coupled to the unpaired electron spin. With ENDOR, nuclear transitions are directly driven using either continuous or pulsed radio-frequency (RF) radiation.[4−7] The effect on the EPR signal as a function of the RF is monitored, and what is obtained is essentially an NMR spectrum of the nuclei that are coupled to the unpaired electron spin. Similar to ENDOR, ESEEM, and HYSCORE are pulse methods that are used to gain information about nuclei in the vicinity of the unpaired electron spin.[7−11] However, unlike ENDOR, in ESEEM and HYSCORE, nuclear transitions are not directly excited. Instead, the timings between the pulses are varied, and the size of either a Hahn or stimulated echo is monitored as a function of time. Similar to the FID signal in an NMR experiment, the time-based data yield a periodic signal dependent on the nuclear Zeeman, hyperfine, and quadrupolar (for $I > 1/2$ nuclei) interactions. A Fourier transform of the time-based data yields a frequency-dependent spectrum similar to that obtained in an ENDOR spectrum, but often with double quantum and combination peaks. The most commonly used ESEEM pulse sequences are the two-pulse and three-pulse sequences.[8,9] HYSCORE is a two-dimensional ESEEM technique in which the peaks are separated into a second dimension, which can often be beneficial for complicated spectra with many overlapping peaks.[11]

Double Electron–Electron Resonance (DEER) or Pulse Electron Double Resonance (PELDOR) Spectroscopy. In systems with two or more EPR active species, there will be an electron–electron dipolar interaction present.[7,12] This interaction depends upon the distance and the angle between the two paramagnetic species relative to the externally applied magnetic field. In DEER spectroscopy, that dipolar coupling is measured, and as a result, the distance between the two species can be accurately determined to be between 20 and 80 Å.[13] This technique has emerged as a very powerful structural biology tool, particularly for site-directed spin-label studies in which the two unpaired electron spins can be engineered into

specific locations in biological macromolecules. A more detailed description of DEER studies on spin-labeled systems can be found below.

■ SPIN-LABEL EPR

Early biological EPR studies were restricted to those systems containing naturally occurring radicals and EPR active transition metals that will be discussed in a later section. However, with the advent of spin-labeling, biological techniques used to place stable radicals at specific locations on biological macromolecules, the potential use of EPR has been extended to nearly any biological system. This is a very broad field of study, and as such, what follows is a basic introduction to the types of experiments and systems in which spin-label EPR is being used. For more in-depth examinations of this topic, the authors direct the reader to several excellent reviews.[1,2,14−19]

The two most widely used techniques for obtaining detailed structural information in biological systems are X-ray crystallography and NMR spectroscopy. These techniques can yield highly detailed structural and in the case of NMR also dynamic information for a variety of biological systems. These methods have their own advantages and limitations. Solution NMR can provide structural information in a physiologically relevant environment but is limited because of size restrictions (approximately ≤50 kDa).[14,20−22] NMR structural studies of membrane proteins are also challenging because of the size of the micelle complex and corresponding increases in line width.[23] X-ray crystallography yields highly resolved structural information but cannot provide detailed dynamic information.[24] In addition, the hydrophobic surfaces associated with membrane proteins often complicate the crystallization process, limiting the use of X-ray crystallographic techniques for many membrane protein systems.[21] EPR spectroscopy has emerged as a powerful technique for overcoming these limitations and provides important solutions to gaining structural and dynamic information about peptides, proteins, macromolecules, and nucleic acids.[1,2,15,16,25−29]

EPR spectroscopy offers high sensitivity (micromolar concentrations), and is not limited by the size of the protein or the optical properties of the sample. EPR measurements can be made on samples ranging from proteins in solution to densely packed membrane suspensions, tissue samples, ammonium sulfate-precipitated solids, or samples frozen and maintained at cryogenic temperatures.[30] EPR measurements are routinely made from approximately 70 nL of a sample at W-band (94 GHz)[31] to several milliliters of a sample or even small animals at L-band (1−2 GHz).[32] EPR spectroscopy can address important structural and dynamic questions related to both solution and membrane-embedded protein systems that are not answered by traditional methods.[1,15,28,33] CW-EPR spectroscopy of spin-labeled molecules reveals structural and dynamic information about the motion of the nitroxide side chain, the solvent accessibility, the polarity of its surrounding environment, and intra- or intermolecular distances between two nitroxides or a single nitroxide and another paramagnetic center in the system.[27] The analysis of the EPR data for a series of spin-labeled protein sequences allows modeling of the protein structure with a spatial resolution at the level of the backbone.[34−37]

Site-Directed Spin-Labeling Methods. Most native biological systems cannot be studied with EPR spectroscopy as they are not naturally EPR active. A reporter group or a label such as a spin-probe needs to be incorporated into the system
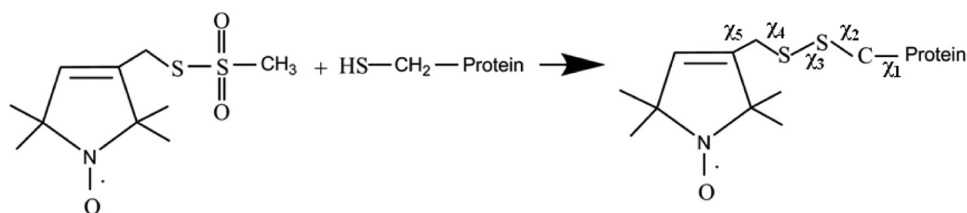
Figure 2. Structure of MTSL and the resulting side chain produced by reaction with the cysteine residue of the protein. χ_1, χ_2, χ_3, χ_4, and χ_5 represent the locations of five rotations about the chemical bonds between the α-carbon backbone of the protein and the pyrroline ring of the attached MTSL.

of interest to be detected by EPR. The site-specific incorporation of unpaired electrons into biomolecules in the form of spin-labels is known as site-directed spin-labeling (SDSL).[38,39] In SDSL experiments, all native non-disulfide-bonded cysteines are eliminated by replacement with another amino acid such as alanine. A unique cysteine residue is then introduced into a recombinant protein via site-directed mutagenesis and subsequently reacted with a sulfhydryl-specific nitroxide reagent to generate a stable paramagnetic EPR active side chain.[27,39,40] Figure 2 shows the structure of the most commonly used spin-label, S-(2,2,5,5-tetramethyl-2,5-dihydro-1H-pyrrol-3-yl)methyl methanesulfonothioate (MTSL), and the resulting side chain produced by reaction with the cysteine residue of the protein.

EPR Structural and Dynamic Information of Biological Systems. The EPR spectra of nitroxide-based site-directed spin-labels are sensitive to the motion of the spin-label and, as such, can be used to observe dynamics within a system.[1] This sensitivity stems from the orientation dependence of both the g values and the hyperfine couplings and the extent to which they are averaged out by the motion of the spin-label. For spin-labels that are moving very rapidly in solution, the spectrum collapses to three sharp peaks. Conversely, if the spin-label motion is very slow such that the spin-label is relatively motionless within the transverse relaxation time for the system, the spectrum is in the rigid limit.[41] In a rigid limit spectrum, it is as if the sample has been frozen and the full orientation-dependent parameters are observed. These "bookends" to the spin-label spectra are determined by the transverse relaxation time (T_2), which in turn determines the range of motional dynamics to which EPR is sensitive. For systems in which the spin-label movement falls between these two extremes, a correlation time, τ_c, can be determined that indicates the dynamic properties of the spin-label at a specific location.[41] The overall mobility of the nitroxide spin-label attached to the protein or peptide is a superposition of the contributions from (1) the motion of the label relative to the peptide backbone, (2) fluctuations of the α-carbon backbone, and (3) the rotational motion of the entire protein or peptide. Under experimental conditions, these motions can be isolated from the EPR spectrum. The spin-label side chain motion is used to study tertiary contacts and protein structure. There are five chemical bonds between the pyrroline ring of the attached MTSL and the α-carbon backbone of the protein (see Figure 2). The flexibility of the MTSL at α-helical sites is dominated by rotations about the two bonds closest to the nitroxide ring moiety (χ_4 and χ_5).[42] The interaction of the disulfide bond with the backbone α-carbon hydrogen restricts the mobility about the first two bonds adjacent to the α-carbon backbone (χ_1 and χ_2). An isomerization about the disulfide bond (χ_3) is slow on the EPR time scale, so that the motion of the MTSL is constrained to isomerizations about χ_4 and χ_5. For β-sheet proteins, the spin-

label motion is influenced by steric interactions with the nearest neighbors.[43] The inverse line width of the central line provides a measure of relative mobility. Scanning the inverse line width of the EPR spectrum against the amino acid sequence yields a periodic data profile that reflects the local secondary structure of the protein.[44] This EPR approach has been routinely used to determine the secondary structure of the protein and peptides (see the review by Klug et al.).[1] This method also provides an efficient strategy for identifying functional domains in high-molecular weight proteins, supramolecular complexes, and membrane proteins.[24] A more detailed description of side chain motion of the spin-label in a biological system can be obtained with EPR spectral simulations such as the microscopic ordered and macroscopic disordered (MOMD) approach.[42,43,45,46]

An excellent example of the application of SDSL−EPR techniques is work done on the *Escherichia coli* ferric citrate transporter FecA.[47] Outer membrane TonB-dependent transporters such as *E. coli* ferric citrate transporter FecA (Figure 3)[48−50] interact with inner-membrane protein TonB through an energy-coupling segment called the Ton box. This FecA protein is involved in ferric iron−iron translocation across the outer membrane. Mokdad et al. determined the position and dynamics of the N-terminal transcriptional domain in FecA using SDSL−EPR methods.[47] X-Band CW-EPR spectra were recorded for several single spin-labeled sites to determine the N-terminal transcriptional motif with and without substrate binding. The more ordered regions of the domain yielded the broadest spectra, while the loop region yielded the narrower spectra with correlation times on the order of 1 ns. No significant spectral differences were observed with and without substrate binding. These results indicated the correct folding of the N-terminal extension with no change in dynamics upon substrate binding. Further spectral analysis indicated that the domains have significant backbone motion on the nanosecond time scale that would be expected for a domain designed for protein−protein interactions. A further study of 10 different spin-labeled sites in the N-terminal transcriptional domain in the absence and presence of PEG 3350 indicated the existence of a conformational equilibrium at these sites.[47] The position of the N-terminal transcriptional domain is not fully resolved in high-resolution crystal structures of FecA. This study also used DEER distance restraints obtained for pairs of spin-labels located on the N-terminal signaling domain and the Ton box or the FecA barrel to determine structural models of the apo, TonB, and substrate-bound states.[47]

Another example of using SDSL−EPR methods to probe the structural and dynamic properties of proteins is Vimentin (Figure 4).[51,52] Vimentin is a type III intermediate filament protein found in many cells of mesenchymal origin. The intermediate filament (IF) gene family includes more than 65 different members, each expressed in a cell-specific or differentiation stage-specific manner. Mutations in IF genes
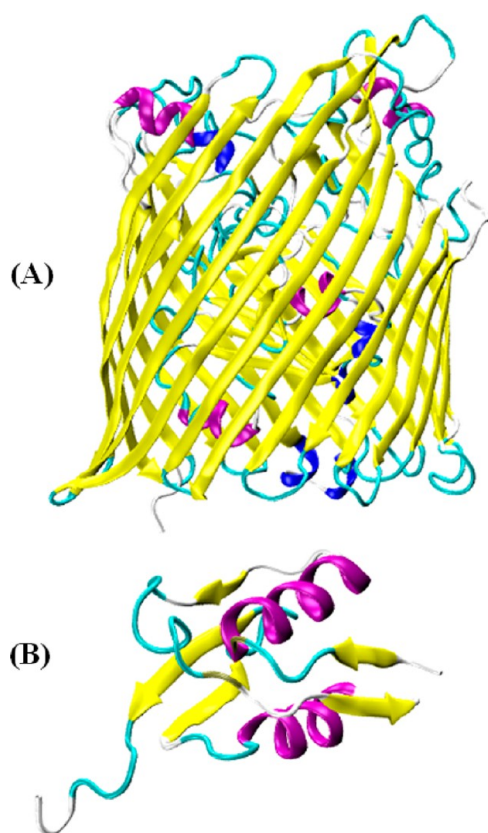
Figure 3. Representation of TonB-dependent iron transporter: (A) X-ray crystal structure of *E. coli* ferric citrate transporter FecA [Protein Data Bank (PDB) entry 1KMO][48] (the N-terminal transcriptional signaling motif was not resolved in FecA) and (B) solution NMR structure of the N-terminal transcriptional signaling motif of FecA (PDB entry 1ZZV).[49] Figures were prepared using VMD.[50]
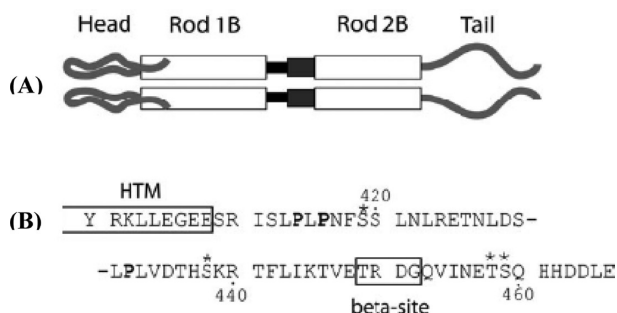

Figure 4. Schematic of the Vimentin molecular structure. (A) Representation of the protein domains of Vimentin. At the amino terminus is the head domain, leading into rod domain 1. The black box between rod 1B and rod 2B represents linker 1−2. The dark gray box between rod 1B and rod 2B represents the parallel helical structure of rod 2A/linker 2. (B) Amino acid sequence of the tail domain, beginning with Y^{400}. The HTM and β (beta) sites are boxed and labeled. Prolines are shown in bold; phosphorylation sites are denoted with asterisks. Adapted from ref 51 with permission.

have been linked to more than 85 different human diseases.[52] Aziz et al. used site-directed spin-labeling X-band CW-EPR data collected at 45 different sites to predict the structural model of the Vimentin head domain.[52] This study also revealed that the Vimentin head domain structure is dynamic and changes with filament assembly. Hess et al. further employed X-band CW-EPR to show that the head and tail domains of Vimentin are

structurally very different and the tail domain undergoes distinctive conformational changes upon assembly with the tetrameric protofilament.[51]

Protein Topology. Membrane proteins play an essential role in controlling bioenergetics, the movement of ions across a cell, and initializing signaling pathways. Membrane proteins can be incorporated into a membrane in several different fashions or orientations. The embedded helices may be short, long, kinked, or interrupted in the middle of the membrane. They may cross the membrane at different angles, lie flat on the surface of the membrane, or form re-entrant loops. Nitroxide-based site-directed spin-labeling EPR can be used to gain pertinent structural and dynamic information about membrane−protein assembly. EPR spin-labels are very sensitive to the presence of other paramagnetic species that alter the relaxation properties.[53] The accessibility of the spin-label to different paramagnetic probes can be used to determine the location of the spin-label in the membrane interior. EPR power saturation experiments can monitor the relaxation rate of spin-labels with extrinsic paramagnetic probes residing in the aqueous phase and in the lipid bilayers by examining the EPR signal intensity as a function of microwave power.[54] The power at which the measured signal amplitude is half-saturated, $P_{1/2}$, is proportional to the longitudinal relaxation rate of the spin-label. When the spin-label is exposed to paramagnetic reagents, the spin−lattice relaxation rate increases, which is dominated by Heisenberg spin exchange.[54] The most commonly used paramagnetic agents in EPR accessibility experiments are lipid soluble oxygen, which serves as a probe for membrane insertion, and polar nickel compounds such as nickel(II) ethylenediaminediacetate (NiEDDA), which is located in the aqueous phase. Nitrogen is used as a control to purge the sample of oxygen during the measurement of the natural longitudinal relaxation rate of the spin-label. There are several biologically important membrane protein systems [e.g., bacteriorhodopsin, ABC cassette transporter MsbA, cytochrome *c* oxidase subunit IV (COX IV), and ferric enterobactin receptor FepA] that have been studied using spin-labeled EPR spectroscopy to investigate structural topology.[54−58] Given the limited format of this review, we are presenting a few recent examples from several studies that are biologically important.

A recent example of using CW-EPR power saturation data is to study the topology of the KCNE1 membrane protein in proteoliposomes.[59] KCNE1 (Figure 5)[60] is a single-transmembrane protein that modulates the activity of the KCNQ1 voltage-gated potassium channel. EPR power saturation data revealed that KCNE1 spans the full width of the lipid bilayer, with the Leu59 residue located near the center of the membrane. Additionally, SDSL−EPR line shape analysis showed that the dynamic motion of the nitroxide spin-label is slower in the membrane environment than in micelles and that residues within the membrane are less mobile than those outside. This information provides an understanding of how KCNE1 is stabilized in a membrane environment more native than micelles.

The accessibility parameters obtained for a series of consecutive sites can also be used to probe the secondary structure.[1] The plot of accessibility parameters against residue number can distinguish α-helical, β-strand, and unstructured regions of a protein. A standard α-helix has a periodicity of 3.6 residues per turn, so every 3 or 4 residues would be highly exposed to the solvent showing high NiEDDA values; the sites on the other side of the helix would be buried against the
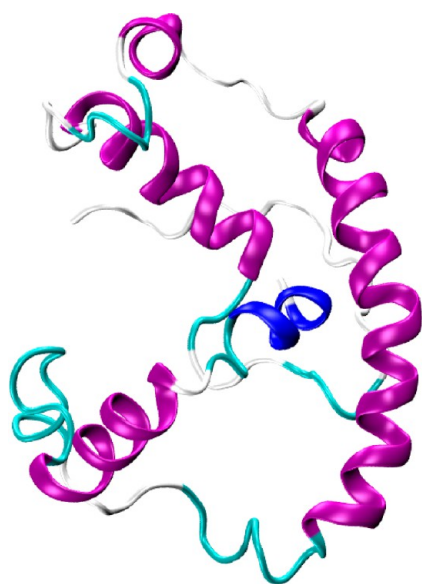
Figure 5. Representation of the NMR structure of KCNE1 membrane protein in LMPG micelles (PDB entry 2K21).[60] This figure was prepared using VMD.[50]

protein, revealing lower values for both NiEDDA and oxygen. Similarly, the β-strand has a periodicity pattern of 2, when compared to a standard α-helix.

An excellent example of using both accessibility data and mobility data to identify the α-helical secondary structure is a study of the lactose permease protein.[61] The X-ray crystal structure of wild-type lactose permease protein is shown in Figure 6.[62] Voss et al. used site-directed spin-labeling EPR to obtain the periodicity of side chain mobility and accessibility to molecular O_2 and concluded that transmembrane domain XII in the lactose permease protein adopts an α-helical conformation.[61] For integral membrane proteins, the depth of
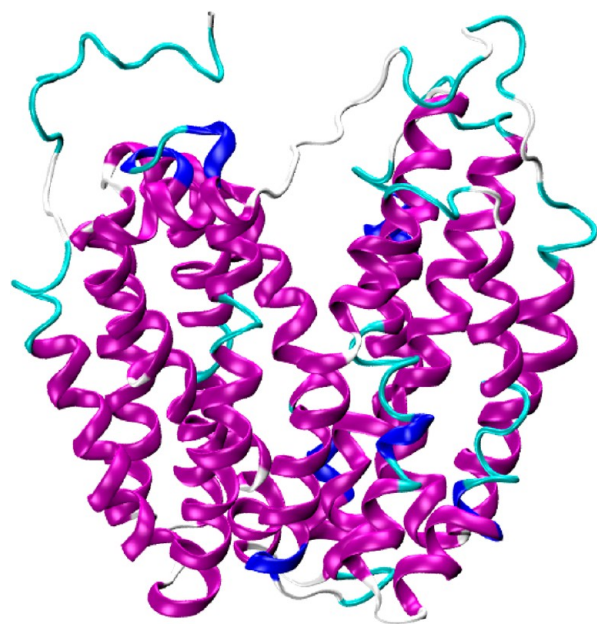

Figure 6. Representation of the X-ray crystal structure of wild-type lactose permease protein (PDB entry 2V8N).[62] This figure was prepared using VMD.[50]

a given spin-label side chain within a lipid bilayer can be determined using accessibility data based on the inverse concentration gradients of oxygen and NiEDDA within a lipid bilayer.[54,59]

CW-EPR spectroscopy at X-band can also be used to study membrane topology of integral membrane proteins inserted into aligned phospholipid bilayers.[63] Recently, Ghimire et al. used the membrane alignment technique coupled with dipolar broadening CW-EPR to determine the distance and relative orientation of two nitroxide spin-labels on the M2δ peptide of the acetylcholine receptor (AchR) in DMPC vesicles.[64]

High-Field, High-Frequency SDSL−EPR Methods. The EPR spectral line shape can provide information about the secondary structure of a protein and the orientation of its subunits relative to each other or to the environment. If the experiment is performed at more than one frequency, it can provide additional information about both the global tumbling of the protein and the internal motion consisting of backbone fluctuations and side chain isomerizations.[65,66] EPR spectral behavior at lower frequency is more sensitive to slower spin motions, whereas spectral behavior at higher frequency is more sensitive to faster spin dynamics.[67] A multifrequency approach supplies snapshots at different time scales but also provides pertinent information from a different angle: hyperfine tensor at lower frequencies and **g** tensor at higher frequencies. Single-frequency spectra can be fit quite easily because of the few parameters that are needed in the EPR spectral simulation. However, EPR spectra recorded at multiple frequencies provide unique perspectives on the molecular motions and therefore, taken together, provide a more complete and accurate description of the dynamics of the spin probe environment.[66] The following three major challenges arise for EPR as a biophysical tool and cannot be resolved by traditional structural methods: (1) structure and dynamics of high-molecular weight proteins in solution, (2) membrane and membrane-associated proteins (structure, location with respect to the membrane, side chain dynamics, and interactions with other membrane components, DNA, or RNA), and (3) fast conformational transitions of proteins and RNAs in solution, protein folding, and refolding. These issues can be more accurately addressed by probing EPR at multiple and higher microwave frequencies.[67] If conventional EPR frequencies (X-band) are extended to higher frequencies, the following five important features emerge:[68] (1) enhanced spectral resolution, (2) enhanced orientational selectivity in disordered samples, (3) enhanced low-temperature electron spin polarization, (4) enhanced detection sensitivity for restricted-volume samples, and (5) enhanced sensitivity for probing fast motional dynamics. At magnetic fields above 3.4 T (95 GHz, W-band), the rhombic Zeeman term provides new information about protein structure and dynamics that cannot be accessed by traditional means.[67] At a frequency of 250 GHz, the slow overall tumbling of large biomolecules is frozen out on the EPR time scale, leaving only the rapid internal modes corresponding to backbone fluctuations in spin-labeled proteins to contribute significantly to the EPR spectrum.[65,69] The additional advantages of extending conventional X-band EPR (9 GHz) to high-frequency EPR include an increased signal-to-noise ratio and a great improvement in the orientational resolution of the nitroxide spectrum.[69] More detailed information about the application of high-field EPR to study biological systems can be found in the literature.[70,71] The following are recent examples of such multifrequency studies.

Multifrequency EPR spectroscopy has provided pertinent structural and dynamic information about myosin.[72] Myosins are a family of ATP-dependent motor proteins. They are involved in muscle contraction and a wide range of other eukaryotic motility processes. An X-ray crystal structure of the motor domain of *Dictyostelium discoideum* myosin II is shown in Figure 7.[73] Nesmelov et al. recorded CW-EPR spectra at X- and

Figure 7. Representation of the X-ray crystal structure of the motor domain of *D. discoideum* myosin II (PDB entry 1FMV).[73] This figure was prepared using VMD.[50]

W-band frequencies on spin-labeled subfragment 1 (S1) of rabbit skeletal myosin for the apo state and in the presence of ADP and nucleotide analogues.[72] Using simultaneous frequency data fits, both the rate and amplitude of restricted motion within myosin were determined and multiple conformational states were resolved in the force-generating region of myosin. This study also provided reliable information about the allosteric influence of nucleotides on multiple conformational states, the relative populations of these states, and the rate and amplitude of spin-label rotation in each state.[72] This study further suggested that the post- and pre-power stroke structural states are in a dynamic equilibrium in solution, even with ADP and vanadate tightly bound to the myosin active site. The molecular events responsible for force generation in a cycling cross-bridge are a major focus of interest in the muscle field.[74] This important study provided the pertinent structure and

dynamic information about the force-generating domain of myosin, addressing a major focus of interest in the field.

Multifrequency EPR has also been used to study the dynamic properties of T4 lysozyme in solution.[66] T4 lysozyme is a globular protein composed of 164 amino acid residues with a molecular mass of 18.7 kDa.[66] Zhang et al. used EPR spectroscopy over a wide range of frequencies (9, 95, 170, and 240 GHz) to obtain dynamic modes of nitroxide side chains in T4 lysozyme.[66] This study demonstrated the power of multifrequency EPR to differentiate the effects of faster internal modes of motion from those of slower overall motions.

SDSL–ESEEM Methods. Electron spin echo envelope modulation (ESEEM) spectroscopy is a very powerful pulsed EPR spectroscopic technique and has been applied to study many different biological systems.[75−79] ESEEM can provide distance measurements up to 8 Å between a spin-label and a single ^{2}H nucleus. Simulations of the spectral data can indicate the number, identity, and radial distance of the weakly coupled nuclei from the electron spin.[7,80] Volkov et al. used ESEEM accessibility data to measure the folding kinetics of the plant light-harvesting complex LHCII membrane protein in a membrane environment.[78] Recently, the Lorigan lab has utilized ESEEM spectroscopy to directly probe the site-specific secondary structure of membrane peptides using microgram amounts of sample.[77,81,82] In this method, a cysteine-mutated nitroxide spin-label is positioned two ($i + 2$), three ($i + 3$), or four ($i + 4$) residues from a fully deuterated Leu chain (i). The characteristic periodicity of the α-helical and β-sheet structure gives rise to a unique pattern in the ESEEM spectra. For $i + 2$ α-helix samples and $i + 3$ β-sheet samples, the ^{2}H nuclei are too far away to be detected. However, with the 3.6-residue per turn pattern of an α-helix, the $i + 3$ samples reveal a strong ^{2}H ESEEM peak from ^{2}H nuclei of the Leu side chain weakly coupled to the spin-label. Similarly, the $i + 2$ sample for a β-sheet can reveal an ESEEM signal from ^{2}H nuclei of the Leu side chain coupled to the spin-label because they are in the proximity of each other. This method has been used to simply and quickly (<1 h) discern the local secondary structure within a protein. Figure 8 shows an example of the three-pulse ESEEM data obtained for AchR M2δ α-helical peptide in a membrane environment and a ubiquitin β-sheet peptide in solution.[77]

Double Site-Directed Spin-Labeling Methods Used To Determine Distances. One of the most active and rapidly developing aspects of EPR spectroscopy is the measurement of distances between two spin-labels in terms of either intramolecular distances on the same protein or intermolecular distances between sites on different proteins.[30] The distance is obtained from the magnetic dipolar interactions between the unpaired electrons of two spin-labels or a spin-label and a paramagnetic metal. Using dual-labeling EPR techniques, distances can be measured to probe secondary, tertiary, and quaternary structures.[30] This method allows the relative orientations between interacting spin-labels to be determined from CW-EPR studies in those cases where a specific orientation exists.[31] The magnetic dipoles of the two spin-labels give rise to a distance-dependent line broadening in the conventional CW-EPR spectrum. CW dipolar broadening EPR can provide pertinent structural and functional dynamic information over an intermediate distance range of 8−20 Å.[83] Recently, the Hyde group extended the upper limit distance measurement to 30 Å at L-band (1−2 GHz) using nonadiabatic rapid sweep electron paramagnetic resonance (NARS EPR).[84] For higher-resolution structural analysis, quantitative distances
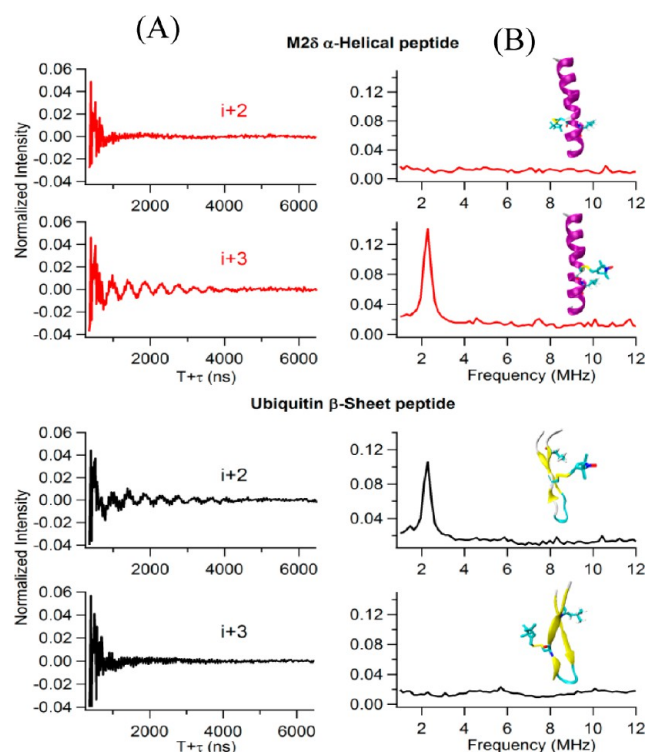
Figure 8. Three-pulse ESEEM experimental data with a τ of 200 ns of the $i + 2$ and $i + 3$ ^{2}H-labeled Leu for AchR M2δ helical peptide in a lipid bilayer and ubiquitin β-sheet peptide in solution: (A) time domain and (B) frequency domain. The inset structural pictures show the location of spin-labels and ^{2}H-labeled Leu on AchR M2δ helical peptide and ubiquitin β-sheet peptide. Adapted from ref 77 with permission.

can be determined using spectral simulations.[31,85−87] The resolution of this method is typically on the order of $\pm 1-2$ Å for flexible spin-labels and 0.1−0.2 Å for highly immobilized, well-oriented spin-labels.[31]

The CW-EPR line broadening approach has been used to study the bacterial K$^+$-translocating protein KtrB.[88] Proteins of this superfamily of potassium transporters are found in archaea, bacteria, fungi, plants, and trypanosomes. They are involved in the uptake of K$^+$ and Na$^+$ by the cells. CW-EPR dipolar broadened data obtained for doubly labeled variants of KtrB in the presence and absence of K$^+$ ions have provided valuable structural models for the open and closed state conformations.[88]

For longer distances, pulsed DEER spectroscopy has proven to be a very powerful and popular structural biology technique for measuring longer-range distances (20−80 Å).[13,89] In DEER, one set of spins are monitored and another set of spins are excited with a second microwave frequency leading to the measurement of the coupling between the two spins and thus the distance between them. DEER can probe the structure of biomacromolecules, globular proteins, membrane proteins, oligomerization states, and RNA.[13,89−94] In addition to measuring distances, DEER at high field can be used to measure the relative orientation of the spins.[95] DEER provides long-range structural distance constraints of the protein backbone and information about the conformational mobility in specific loop regions.[96] However, in some cases, the high effective concentration in the two-dimensional environment of membrane systems develops a strong background contribution

imposing severe limits on sensitivity, distance range, and experimental throughput.[97] Recent studies have reported an increase in sensitivity in DEER measurements for proteins when the experiment was performed at Q-band when compared to X-band.[98−101] Also, Hubbell and co-workers have used a rigid nitroxide side chain RX to minimize the spin-label motion for more accurate distance measurements.[102] The RX side chain can be generated by a facile cross-linking reaction of a bifunctional methanethiosulfonate reagent with pairs of cysteine residues at positions i and $i + 3$ or i and $i + 4$ for an α-helix and at positions i and $i + 2$ for a β-strand, or with cysteine residues in adjacent strands in a β-sheet. The protein fluctuation dynamics and spin-label rotameric motions make a significant contribution to the DEER distribution width. With the development of molecular dynamics simulations, recently Jao et al.[103] and Hirst et al.[104] have used DEER distance restraints to refine the secondary structure of membrane-associated proteins. These methodological developments have made DEER a powerful spectroscopic tool for solving several pertinent biological problems.

DEER has been used to identify the curved α-helical nature of the transmembrane region of the C99 amyloid precursor protein in proteoliposomes as shown in Figure 9.[105] C99 is a transmembrane carboxyl-terminal domain of the amyloid precursor protein that is cleaved by γ-secretase to release amyloid-β polypeptides that are involved in Alzheimer's disease. Two MTSL spin-labels were generated at the ends of the transmembrane domain (TMD) of C99 (residues 700−723). The dual-spin-labeled C99 protein was reconstituted into LMPG micelles and POPC/POPG liposomes. The distance distributions were obtained by analyzing the time evolution DEER data. The identical distances obtained for both LMPG micelles (33.5 $\pm$ 1.2 Å) and POPC/POPG liposomes (34.5 $\pm$ 0.5 Å) verify that the TMD attains similar curvature in liposomes and in micelles. The curved nature of the TMD is very important for interactions of C99 with γ-secretase. Additionally, CW-EPR power saturation data were used to conform the spanning of TMD of C99 and revealed that the N- and C-helices are associated with the membrane surface.

Another recent example using SDSL−EPR distance methods is on the cardiac Na$^+$/Ca^{2+} exchange (NCX1.1) system.[106] The cardiac Na$^+$/Ca^{2+} exchange protein is an antiporter membrane protein that removes calcium from cells. The exchanger is regulated by binding of Ca^{2+} to its intracellular domain, which contains two homologous Ca^{2+} binding domains (CBD1 and CBD2). NMR and X-ray crystallographic studies have provided the structures for the isolated CBD1 and CBD2 domains and the corresponding effect of Ca^{2+} binding on their structures and motional dynamics. However, structural information was not obtained for the entire Ca^{2+} binding domain (CBD12) and the effect of Ca^{2+} binding on its structure and dynamics. These questions were addressed using SDSL−EPR methods.[106] EPR measurements on singly labeled constructs of CBD12 were used to identify the regions that undergo dynamic changes upon Ca^{2+} binding. DEER measurements on a dual-labeled construct of CBD12 indicated that the β-sandwich regions of the CBD1 and CBD2 domains are widely separated at their N- and C-termini and are largely insensitive to Ca^{2+} binding. Additionally, the authors used DEER distance restraints to construct structural models for CBD12 in the absence and presence of Ca^{2+}.[106] These structural models indicated that there is not a major change in the relative orientation of the two
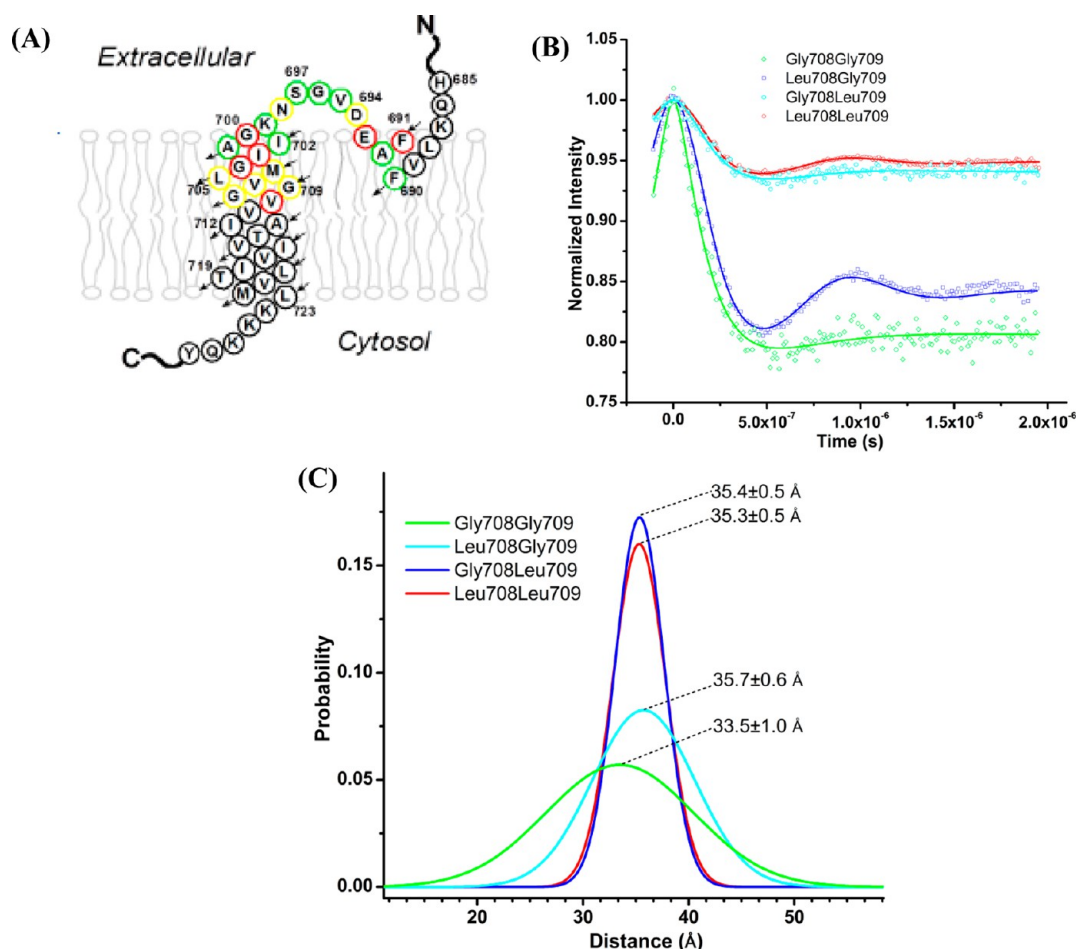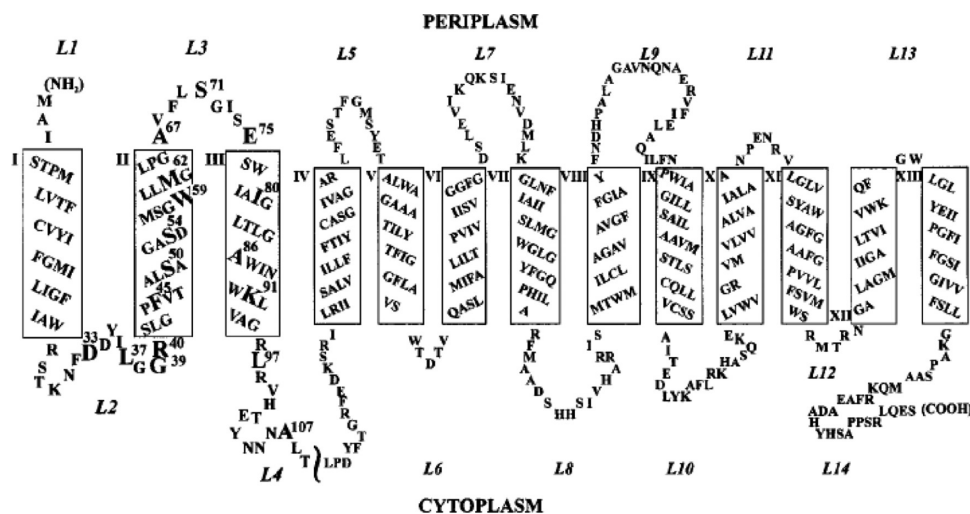
Figure 9. DEER data used to identify the curvature helicity of the transmembrane region of amyloid precursor protein (C99) in a POPC/POPG vesicle system. (A) Topological illustration of C99 with respect to a lipid bilayer. (B) X-Band DEER time domain data at 80 K for C99 that was spin-labeled at the ends of its TMD (at sites 700 and 723). Data are shown for WT C99 and also C99 that was additionally subjected to Gly-to-Leu mutations at G708 and G709. (C) Distance distributions between the spin-labels measured for the corresponding time domain data. The error associated with each average distance relates to the uncertainty of the average. Adapted from ref 105 with permission.

Figure 10. Secondary structure model of Na⁺/proline transporter PutP of *E. coli*. Putative TMs are represented as rectangles and numbered with Roman numerals; loops are numbered with Arabic numerals starting from the N-terminus. Adapted from ref 110 with permission.

Ca²⁺ binding domains as a result of Ca²⁺ binding in the NCX1.1 isoform.

Another excellent example for measuring distance constraints with DEER spectroscopy is the Na⁺/proline transporter PutP *E.*

coli system.[107] Na⁺/proline transporter PutP of *E. coli* is a prokaryotic member of the sodium solute symporters (SSS) family. Proteins of this family utilize a sodium motive force to drive uphill transport of substrates such as sugars, amino acids,

vitamins, ions, myoinositol, phenyl acetate, and urea. A secondary structure model of Na$^+$/proline transporter PutP of *E. coli* (Figure 10) has been predicted on the basis of a gene fusion approach, Cys accessibility analysis, site-directed spin-labeling, and site-specific proteolysis.[108−110] Hilger et al. used SDSL−DEER distances to determine the backbone structure of transmembrane domain IX of Na$^+$/proline transporter PutP of *E. coli*.[107] Transmembrane (TM) domain IX appears to line the translocation pathway and is involved in ligand binding and transport. DEER distance distribution measurements for 16 pairs of spin-labels were used in helix−loop−helix modeling to predict the kinked helical structural models of TM domain IX of PutP. The kink in the TM domain is associated with a hinge that allows the protein to open and close during substrate binding.[107] DEER has also been successfully used to study the tetrameric potassium ion channel KcsA to measure pertinent distances and the orientation of the spin-label.[111] The examples discussed above clearly show the power of SDSL−DEER techniques to solve significant biological problems.

Protein−Protein Interactions. Protein−protein interactions are involved in almost all biological processes such as immune responses, cell signaling, translocation, and regulation.[112] EPR spectroscopy is a powerful technique for studying protein−protein interactions and oligomerization states.[1,113] When a spin-labeled molecule is mixed with its binding partner, the EPR spectrum constitutes a linear combination of spectra representing the bound and unbound components. The fraction of each state can be extracted by the numerical decomposition of the spectrum.[113] DEER spectroscopy has emerged as a very powerful tool for measuring the distance between two spin-labeled binding sites in a protein−protein complex.[114,115] A detailed application of site-directed spin-labeling EPR for studying protein−protein interactions can be found in previous reviews.[1,14]

A recent example of the application of CW-EPR and DEER spectroscopy to study complicated protein−protein complexes is the interaction of cdb3/AnkD34 proteins.[114] The ankyrin family of adaptor proteins serves critical functions in cells by linking the lipid bilayer to the spectrin-actin-based membrane skeleton as well as assembling proteins in specialized membrane domains. CW-EPR and DEER spectroscopy were used to map the binding interfaces of these two proteins in the complex and to obtain interprotein distance constraints to build a structural model.[114] Another good example is the ATP-binding cassette transporter in association with antigen processing (TAP), which participates in the adaptive immune defense against infected or malignantly transformed cells. This system translocates proteasomal degradation products into the lumen of the endoplasmic reticulum for loading onto MHC class I molecules. Herget et al. used CW-EPR spectroscopy to reveal conformational details of the bound peptides and DEER spectroscopy to determine distances in dual-labeled peptides bound to TAP.[116] Also, James et al. used saturation transfer electron paramagnetic resonance (ST EPR) spectroscopy to probe the homo- and hetero-oligomeric interactions of the sarcoplasmic reticulum Ca-ATPase (SERCA) and phospholamban (PLB).[117]

■ UNPAIRED SPINS IN BIOLOGICAL SYSTEMS

Many systems in nature contain unpaired electron spin and as such can be studied natively using EPR methods. These systems range from enzymes that function via transient radical intermediates to those containing stable unpaired electron spins

and transition metals. Because the electrons being observed often participate intimately in biological processes, EPR methods can reveal pertinent structural information for these systems. In this section, because of the significant overlap of EPR techniques used to examine naturally occurring radicals and transition metals, we survey selected examples of organic radical-based and transition metal-based systems that offer illustrative examples of the biological questions that can be answered using EPR spectroscopy.

Naturally Occurring Radicals. Throughout nature, organic-based radicals are utilized in enzymatic reactions and electron transport. Some can be persistent, like the tyrosine residue (Y_D) in photosystem II, but most cycle as part of the function of the system and as such can be short-lived. The most common biological radicals are those stemming from amino acid residues such as tyrosine and tryptophan, cofactors such as flavins, and pigment molecules such as chlorophylls.[118] These systems typically contain one unpaired electron spin residing most often in an aromatic molecular orbital. Organic systems containing one unpaired electron spin rarely have g values that deviate substantially from that of a free electron, and as such, at the most common frequency used in EPR, X-band (9 GHz), the EPR spectra are typically dominated by hyperfine interactions. Because of this, it can often be difficult to resolve any small orientation dependence that is present in the g values using typical EPR spectrometers. However, access to higher-field, higher-frequency instruments is becoming more common, and as such, these small anisotropies in the g values are being determined more frequently.[118,119] The deviation of the g values can be characteristic of a given system, and as such, they can be used to gain information about the identity and environment of the electron spin. In cases where the g values can be resolved, the span and skew for the spectrum can be determined on the basis of the canonical g values. These values give the breadth and overall symmetry of the signal.[118] The various commonly observed biological radicals give relatively characteristic values, and as such, the high-field EPR spectrum can indicate the origin of a radical where a typical X-band EPR spectrum would not be able to resolve any g values, rendering these different radical systems indistinguishable. In the following sections, we will show several illustrative examples of how EPR and related methods have been used to answer important biological questions in systems containing organic-based biological radicals. For a more extensive treatment of this topic, we refer the readers to a recent review by Stoll.[118]

Phycocyanobilin:Ferredoxin Oxidoreductase (PcyA). Phycocyanobilin:ferredoxin oxidoreductase (PcyA) catalyzes the reduction of biliverdin to (3Z/3E)-phycocyanobilin via a four-electron process.[119−121] The conversion of biliverdin to a variety of other compounds that have wide ranges in light absorption profiles allows cyanobateria to capture a range of light greater than that captured by plant systems. This system functions via a two-step, four-electron reduction with 181,182-dihydrobiliverdin (DHBV) as the intermediate in the reaction. It was shown that this process proceeds via short-lived radical intermediates (on the time scale of minutes) and that long-lived, stable radical intermediates could be produced with certain mutations near the active site of the enzyme. Because no significant DHBV was detected in these mutant systems, it was likely that the trapped intermediate corresponded to the one-electron-reduced biliverdin intermediate.[119−121]

As mentioned above, the small amount of g anisotropy present in many biological radicals precludes the precise

determination of the g values by conventional low-field, low-frequency EPR. Such is the case for the radical intermediate in the PcyA reaction as can be seen in Figure 11. The X-band (9.6
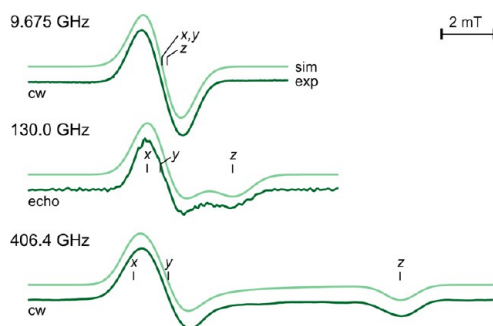

Figure 11. EPR spectra and corresponding simulations at three fields and frequencies of the radical intermediate in the phycocyanobilin:-ferredoxin oxidoreductase system. As the frequency increases, what is an isotropic signal at X-band eventually becomes much better resolved, allowing for the determination of all three g values. Reproduced with permission from ref 119. Copyright 2009 American Chemical Society.

GHz) EPR spectrum of the PcyA intermediate is very nearly isotropic. However, at D-band (130 GHz), the signal is axial with poorly resolved g_x and g_y values. At a very high field and frequency (406 GHz), the signal is still somewhat axial, but the g_x and g_y values exhibit greater separation. A simulation of the high-field spectrum was able to extract the three principal g values with a great deal of certainty. While these results are informative, they do not yield information regarding the orientation of these g values with respect to the molecular frame. To elucidate the orientation of the g values, the researchers undertook a series of single-crystal rotation experiments. In these experiments, collected at D-band, three samples were prepared each aligned along one of the principal crystallographic axes. Successful simulation of the data determined the orientation of the principal g values in relation to the molecule frame. With the g values and orientation in hand, the researchers undertook a series of density functional experiments using all possible protonation states for the radical intermediate. Density functional calculations use a quantum mechanical approach to determine a molecular orbital model from a particular basis set and molecular structure. This quantum mechanical model can help predict the EPR parameters such as hyperfine couplings and the magnitude and orientation of the principal g values. The primary factor that gives rise to deviations in g values away from that of the free electron value is spin orbit coupling within the molecule. Spin orbit coupling is the interaction between the unpaired electron spin and low-lying unoccupied excited states. Spin orbit coupling for a given degree of electron spin density on an atom increases as the atomic number increases, and as such, oxygen atoms within a molecule typically dominate the spin orbit coupling in organic biological radicals. When the predicted parameters from these calculations were compared with the values obtained from the high-field and single-crystal EPR studies, it was determined that the radical intermediate in the reaction was likely protonated at both the A- and D-ring carbonyl oxygens. This prediction carried with it mechanistic implications. The suggested protonation states consistent with the EPR data suggest a proposed mechanism in which one of the intermediates in the first two-electron reduction step consisted of a cationic radical with both terminal oxygen atoms

in a protonated state. This study offers a powerful example in which the combination of EPR techniques has shed light on the chemical mechanism of an important biological system.[119]

Ribonucleotide Reductase. Perhaps the most well-characterized naturally occurring radicals (tyrosine, tryptophan, and cysteine) are those in the various forms of the ribonucleotide reductase (RNR) family of enzymes.[122] The RNR family of enzymes catalyzes the conversion of ribonucleotides to the deoxyribonucleotides that are used in the synthesis of DNA in every living organism. In this review, we will focus on the class 1 RNR systems that consist of two subunits, R1 and R2. The ribonucleotide reduction reaction is thought to proceed via the creation of a tyrosine radical in the R2 subunit by the diiron center in the R1 subunit, followed by an electron transfer reaction creating a thiyl radical near the substrate binding site and the subsequent reduction of the ribonucleotide.[123] This radical was first identified not by the high-field methods described above but by monitoring the change in the EPR signal following the isotopic ^2H labeling of the β-proton positions of the tyrosine residues in the system.[124,125] At the time, high-field EPR instruments were not common, and as such, a detailed analysis of the signal was not conducted until years later. As in the case of the PcyA system discussed above, eventually, EPR examinations of this system have benefited greatly from high-field, high-frequency investigations.[126−128] High-field single-crystal EPR methods were used to determine both the precise canonical g values and the orientation in crystals that had been soaked in H_2O_2 to generate the radical intermediate (Figure 12).[127] The results showed that the tyrosyl group was tilted slightly when compared to the results from the resting state crystal structure, suggesting that the formation of the radical is accompanied by the loss of a hydrogen bond and a shift of the position of the residue that could prove to be critical in the shuttling of hydrogen atoms to and from the residue.[127]

In addition to the information that the g values have provided, the determination of the various hyperfine interactions within the tyrosine radical has yielded insight into the function of the system. The two β-protons of the tyrosine radical in RNR have isotropic hyperfine interactions that are sensitive to the dihedral angle of that position in the molecule and as such have been a good reporter of structure. These hyperfine interactions are difficult to resolve in the EPR spectra; however, they can be directly observed by techniques such as ENDOR. The examination of these hyperfine interactions led to the discovery that several RNR enzymes from different organisms show a variance in the hyperfine pattern for these two β-protons. Differences in these hyperfine couplings have correlated with differences in the allosteric regulation of the various classes of RNRs. This suggests varying local structures for the tyrosine radical might have important implications for tuning the reactivity of the enzyme.[129]

Other Important Biological Systems. While the short format of this review precludes a significant overview of the literature, we would like to mention several other systems in which EPR has been used to help solve pertinent biological problems. Quinone-based electron transport systems have been extensively studied using EPR and ESEEM, and these studies have helped shed light on the important Q-cycle in the complex III family of membrane-bound electron transport systems.[130] EPR methods have also been used to further the understanding of the roles of the two redox active tyrosine residues within
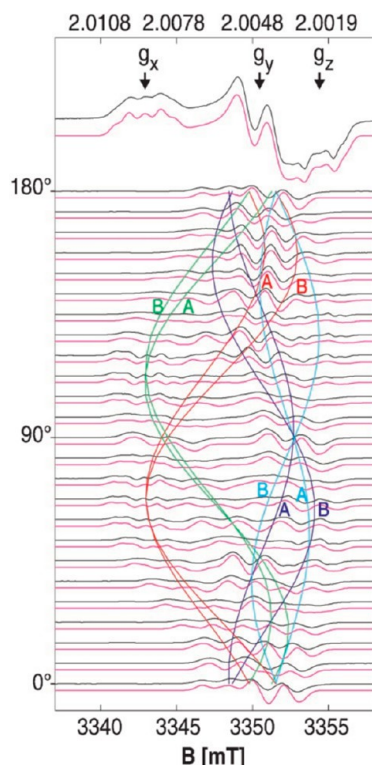
Figure 12. These data show the single-crystal rotation of the H_2O_2-induced tyrosine radical intermediate in ribonucleotide reductase. From the results, the researchers were able to determine the orientation of the tyrosine side chain within the crystal, which is slightly rotated from X-ray diffraction structure of the resting state. Reproduced with permission from ref 127. Copyright 2003 National Academy of Sciences.

Figure 13. X-ray crystal structure of the metalloenzyme core of the oxygen-evolving complex (PDB entry 3ARC).[133] Atoms are colored as follows: Mn, purple; Ca, yellow; O, red. This figure was prepared using VMD.[50]

photosystem II.[131] Many biological cofactors have also been studied using EPR such as chlorophylls, flavins, and others.[118]

Metals in Biological Systems. Each year, more and more biological systems that depend on metals for proper function are discovered. These metals can play structural roles but more often participate in redox reactions and electron transfer. As in the previous section, this topic could easily fill a textbook. As such, we will focus on several illustrative examples in which EPR was used to answer difficult questions in metalloenzymes.

Oxygen-Evolving Complex (OEC) in Photosystem II (PSII). Photosystem II is a multisubunit membrane-associated enzyme system that catalyzes the light-driven oxidation of two molecules of water to molecular oxygen, releasing four protons that help fuel the pH gradient that drives ATP synthesis and four electrons in the form of reducing equivalents that eventually participate in the reduction of carbon dioxide to sugar. This reaction proceeds in a light-driven fashion in which the absorption of individual photons causes the stepwise oxidation of the OEC and the concomitant release of molecular oxygen. The pattern of this cycle was first described by Kok as a series of five "S" states in which S_1 is the dark stable state and S_4 spontaneously decays to S_0, releasing oxygen. The water oxidation chemistry occurs at the OEC that consists of four Mn atoms and one atom each of calcium and chloride (Figure 13).[132,133]

In the early 1980s, an EPR signal was discovered in chloroplast membranes that had been exposed to a single high-intensity laser flash.[134,135] The multiline signal ($g = 1.96$) consisted of approximately 16 hyperfine lines and was similar to
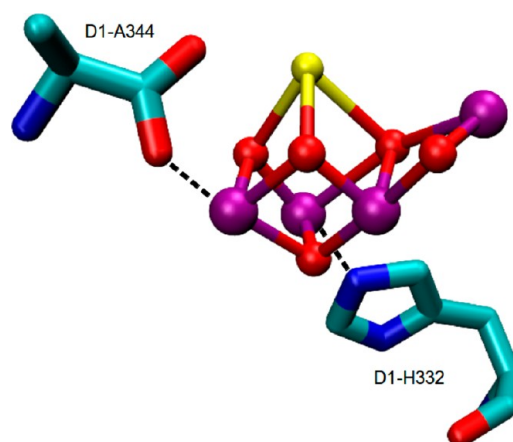
that which had been observed in Mn dimer compounds with bridging oxygen ligands. While it was known that the Mn within the system was essential for water oxidation, the similarity of this light-induced spectrum with that of dinuclear Mn compounds shed light on the possible structure of the cluster. The ground state of the species in the S_2 state that gives rise to the multiline signal was determined to arise from an $S = \frac{1}{2}$ ground state, meaning that the coupling of the Mn atoms within the cluster was such that there was only one net unpaired electron in the ground state molecular orbital. The span of the spectrum, when compared to those of the Mn model compounds, suggested that there were possibly more than two Mn ions giving rise to the multiline signal. In addition to the multiline signal, a second signal at $g = 4.1$ was discovered that arose from a separate $S = \frac{5}{2}$ species.[136−139] The discovery and analysis of hyperfine lines in the $g = 4.1$ signal in the presence of ammonia suggested that all four Mn atoms participated in both the $g = 4.1$ signal and the multiline signal and suggested that the two signals stemmed from two separate electronic states of the OEC that were in equilibrium.[140] It has recently been suggested that this interconversion between the multiline and $g = 4.1$ signals could involve a shift within the bridging oxygens of the OEC from one Mn to another.[141]

Several years later, another multiline signal was discovered that was associated with the S_0 state of the OEC.[142,143] Like the signal associated with the S_2 state, this signal was centered near $g = 2$ and had an appearance similar to that of Mn dimer compounds. The presence and appearance of these two multiline signals, separated by two laser flashes, provided a great deal of evidence of Mn-centered oxidation on the S_0-S_1 and S_1-S_2 transitions as well as the potential oxidation states of the Mn within those states.

In addition to the traditionally detected perpendicular mode EPR signals discussed above, a signal was discovered for the S_1 state in parallel detected EPR experiments.[144] Parallel mode EPR has different selection rules and, as such, can detect transitions that perpendicular mode EPR cannot. It is typically used to observe integer-spin systems that would otherwise be EPR silent. This signal was again shown to arise from the OEC based on observed hyperfine interactions.[145] In all, each of the S states with the exception of S_3 and S_4 (which has not been trapped because of its short-lived nature) has been charac-

terized by EPR spectroscopy with insight into the nature of each of the catalytic steps gleaned from the data.

While EPR spectra can sometimes detect interactions between an unpaired electron spin and other electrons and nuclei in their vicinity, those interactions are often lost in the large inhomogeneously broadened EPR spectra of transition metal systems. To observe these interactions, it is often necessary to use more sophisticated pulse and CW-EPR methodologies. Several of these methods have been very useful for examining the environment of the OEC, particularly ESEEM and ENDOR.

The multiline signal associated with the S_2 state of photosystem II has been investigated with ^{55}Mn ESE-ENDOR.[146,147] The pattern of multiline signal arises from the coupling between the $S = ^1/_2$ electron spin and all of the nuclei in its vicinity, with the isotopically prevalent ^{55}Mn $I = ^5/_2$ nucleus being the dominant interaction. Coupling to the four Mn atoms within the cluster gives rise to 1296 (6^4) potential transitions at a given orientation. This is further complicated by the anisotropy in the **g** tensor and the hyperfine parameters for each of the four Mn nuclei. These essentially infinite numbers of transitions overlap, giving the relatively information poor line shape that consists of 18−20 features. As such, the interpretation of this spectrum led to several sets of hyperfine parameters that each adequately fit the experimental data, each having different consequences for the electronic and chemical structure of the OEC.[148−150] In an impressive set of experiments, the Britt laboratory removed the ambiguity in these various parameter sets by conducting a series of high-frequency ^{55}Mn ENDOR experiments. The hyperfine coupling between the unpaired electron spin and the four Mn atoms is quite strong and much larger than the ^{55}Mn Larmor frequency at X-band. This means that in the ENDOR spectrum, the appearance will be dominated by the hyperfine interaction, with peaks occurring at half the hyperfine coupling. This gives rise to the ENDOR spectra shown in Figure 14. These spectra allowed the simultaneous fitting of both the relatively information poor CW-EPR spectra along with the ^{55}Mn ENDOR spectra. While there were multiple interpretations that could adequately fit the CW-EPR spectra, only one of the sets of values also fits the ^{55}Mn ENDOR spectrum. When combining the hyperfine coupling pattern (factoring in the projection factors based on the oxidation states of the Mn) and the J couplings between the antiferromagnetically coupled oxo-bridged Mn atoms, the researchers came up with a proposal of a strongly coupled trinuclear core with a third more weakly coupled Mn and the possible arrangements of the oxidation states of the Mn within the cluster. These interpretations were verified when crystal structures emerged with a rough trimer−monomer pear shape to the electron density.[151] This study demonstrated the powerful potential of EPR to yield structural information for complicated multinuclear clusters. Recently, a higher-field ^{55}Mn ENDOR study has been conducted in both the S_0 and S_2 states with structural implications discussed in light of a recent high-resolution crystal structure.[152]

In addition to the studies mentioned above, ESEEM and ENDOR techniques have been very powerful in determining ligand identity to the OEC. Through ^{15}N-labeled ESEEM experiments, it was shown before any crystal structures were present that a histidine residue was directly ligated to the cluster.[153,154] Further experimentation over the years involving multifrequency ESEEM studies has shed light on the hyperfine couplings of the directly bound and second nitrogen of the
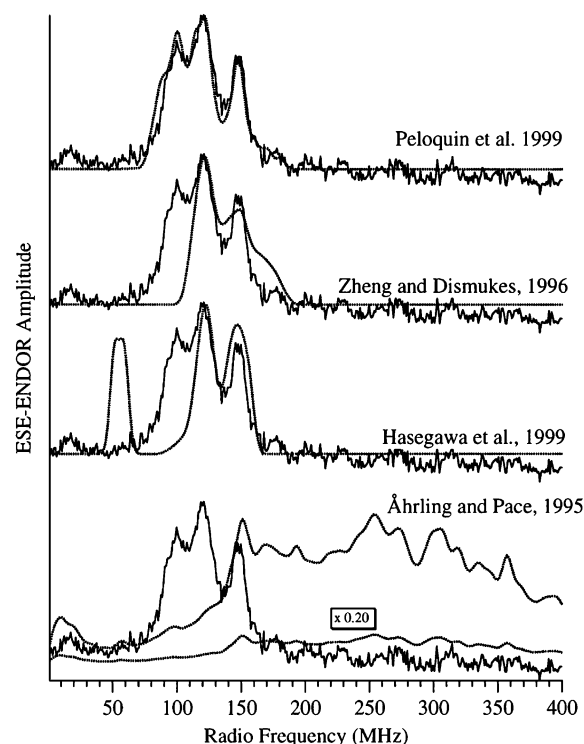

Figure 14. Shown in this figure are the ^{55}Mn ESE ENDOR data collected by the Britt laboratory and the corresponding simulations using the hyperfine parameters from various predictions based on the multiline signal. The utility of using combined EPR methods is apparent as each of these sets of parameters can adequately simulate the multiline EPR signal in the S_2 state of the OEC, and only the Britt values can be used to adequately simulate the ^{55}Mn ESE ENDOR spectrum. Reproduced with permission from ref 147. Copyright 2000 Annual Reviews.

imidazole ring and the nature of the histidine ligation to the OEC.[155−157] More recently, controversy about whether the C-terminal end of the D1 protein was directly ligated to the OEC was settled with EPR methods. Detection of a ^{13}C coupling in samples prepared with alanine labeled with ^{13}C at the carboxylate position provided direct evidence of the many Fourier transform infrared examinations that had suggested this ligation.[157,158] In addition, preparing samples with ^{2}H-labeled water or ^{17}O-labeled water has allowed EPR to determine how many waters are bound at the various states within the S cycle.[159,160] Careful analysis and simulation of the ENDOR and ESEEM data of PSII poised in the S_2 state with ^{1}H- or ^{2}H-labeled water led to the suggestion that one water molecule was likely directly ligated to the cluster with a second at a longer distance, possibly ligated to the Ca within the OEC.[159]

FeMo Cofactor of Nitrogenase. Nitrogen fixation is the process by which N_2 is reduced to two molecules of ammonia and is catalyzed by an enzyme system known as nitrogenase. This system consists of two parts, an electron delivery system, the Fe protein, which delivers an electron upon the hydrolysis of two molecules of ATP, and the second part, the FeMo protein, which contains an iron−molybdenum cluster in which catalysis takes place.[161,162] Figure 15 shows the X-ray crystal structure of the FeMo cofactor of nitrogenase.[163] Despite intense work for decades, there are still many unanswered questions about this complex system. However, EPR methods have shed light on much of what is known about this system. As with PSII, many of the intermediate states have EPR spectra
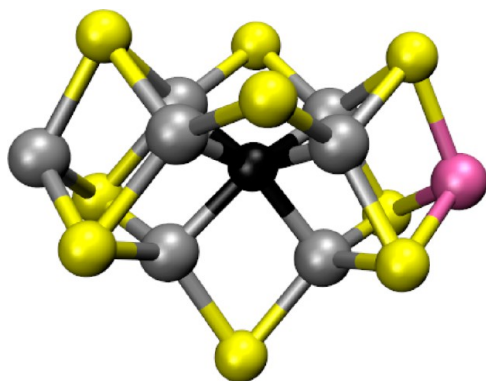
Figure 15. X-ray crystal structure of the FeMo cofactor of nitrogenase (PDB entry 3U7Q).[163] Atoms are colored as follows: Mo, magenta; Fe, silver; S, yellow; interstitial light atom, black. This figure was prepared using VMD.[50]

that by themselves are informative and also allow techniques such as ENDOR to be used to further characterize the system. There are a large number of EPR spectra that have been generated from the Fe and FeMo proteins after then have been subjected to different conditions. Of greatest interest is the FeMo cluster in which the nitrogen fixation chemistry occurs. As isolated, this cluster exists as a rhombic $S = \frac{3}{2}$ system with g values of 4.32, 3.64, and 2.00.[164] However, most importantly, these EPR signals associated with the nitrogenase system yield unpaired electron spins that can be used for techniques such as ESEEM, ENDOR, and HYSCORE.

Several of the substrates and inhibitors that bind to the FeMo cluster have been characterized in various states using ENDOR by the Hoffman lab. Of great interest are the natures of the intermediate states in the reaction, as they represent snapshots of the chemistry that is occurring during the reduction of N_2. The first study that we will discuss is an EPR–ENDOR examination of the CO-inhibited state. This state is produced under turnover conditions in a CO atmosphere and has two signals that appear depending on the CO pressure. The results of this study showed that one CO molecule bound to the cluster at low CO pressures, while two were bound at high pressures. These results were accomplished by using ^{13}CO.[165,166] Because of the strong g anisotropy of the EPR signal, both the isotropic and anisotropic components of the hyperfine interactions were determined. When the g anisotropy is well-resolved, techniques like ENDOR can be conducted as a function of the magnetic flied across the EPR envelope. The resulting ENDOR spectra show single-crystal-like orientation dependencies that can allow both the determination of the anisotropic hyperfine interactions and their orientation compared to the g value frame. When the results for the low-pressure system were compared to those of other CO-M bound systems, it was determined that there was likely a single CO molecule bridging two Fe atoms via the ^{13}C atom. When the pressure was increased, two CO molecules were detected that were bound to Fe atoms within the cluster through the ^{13}C atoms in a nonbridging arrangement. They were also able to suggest the likely location of the binding as the "waist" portion of the FeMo cluster.[165]

Studies of inhibited intermediates occurred first because of their relative ease of preparation. However, true intermediates along the N_2 reaction pathway were more difficult to prepare as they are typically very short-lived. To trap some of these

intermediate states, researchers used a clever combination of targeted mutations, rapid freeze quench techniques, and isotopic substitutions. By creating several key mutations, supplementing the sample with various intermediate state analogues and freeze quenching the system under turnover conditions, the researchers were able to examine their interaction with the FeMo cluster. Several EPR methods were combined to give insight into the intermediate states and the general reaction pathway. The researchers used a double mutant of the enzyme that allows the system to be trapped in an intermediate state.[167] They then used three different substrates ($^{15}N_2H_4$, $^{15}N_2H_2$, and $^{15}N=N-CH_3$) (MD) and characterized the trapped intermediate with each of these substrates using ^{15}N ReMims ENDOR (Figure 16). The results
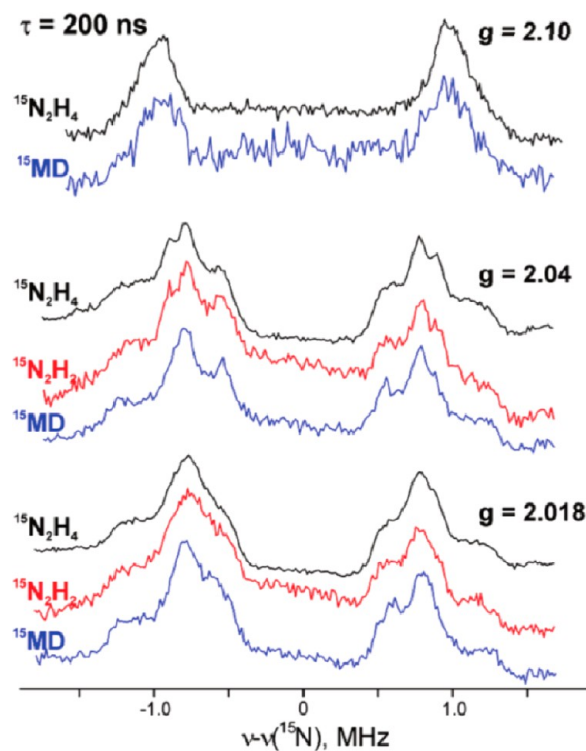

Figure 16. ^{15}N ReMims ENDOR spectra of a trapped intermediate state in the nitrogenase enzyme with $^{15}N_2H_4$, $^{15}N_2H_2$, or $^{15}N=N-CH_3$ (MD). The data show a single intermediate common to each of the added substrates. Adapted with permission from ref 167.

showed that each of these substrates shared a common trapped intermediate state. This was taken as evidence that each of these intermediates plugs into the common reaction pathway from N_2 to $2NH_3$. These results also suggest that the most likely reaction pathway for nitrogen fixation is used in a manner in which protons are added alternately to each nitrogen from N_2 as opposed to the so-called "distal" mechanism in which three protons are added to the first nitrogen, releasing one molecule of NH_3 followed by the hydrolysis of the second nitrogen.

Metal Replacement. While there are large numbers of EPR active metal-based systems within nature, there are still many that are EPR silent because of the identity of the metal. Of particular importance in nature are Mg and Zn. Many systems require Zn for function. Because $Zn(II)$ is a d^{10} system, there are no unpaired electrons to study using EPR. However, many of these systems can be functionally substituted with

Co(II), giving an EPR active probe within the system. One important biological system that has been studied in this manner is the metallo-β-lactamase family of enzymes.[168,169] These enzymes are a primary target for antibiotic drug design and have been well characterized by the replacement of Zn(II) with Co(II) for EPR studies. Another system in which metal replacement has allowed for extensive EPR studies is the interaction of nucleic acids with Mg^{2+}. While Mg^{2+} is EPR silent, it can be functionally replaced with Mn^{2+}, giving a spectroscopic probe that has been extensively utilized to help understand the role of the counterion in the structure and function of nucleic acids.[170]

CONCLUSION

In this review, several key examples were provided to show biological researchers that EPR spectroscopy is a powerful biophysical technique that can be used to answer important biological questions. EPR spectroscopy can be used to complement existing structural biology methods or provide pertinent information when traditional techniques cannot be used.

AUTHOR INFORMATION

Corresponding Author
*E-mail: gary.lorigan@miamioh.edu. Telephone: (513) 529-2813. Fax: (513) 529-5715.

Notes
The authors declare no competing financial interest.

REFERENCES

(1) Klug, C. S., and Feix, J. B. (2008) Methods and Applications of Site-Directed Spin Labeling EPR Spectroscopy. *Methods Cell Biol. 84*, 617−658.

(2) Fanucci, G. E., and Cafiso, D. S. (2006) Recent advances and applications of site-directed spin labeling. *Curr. Opin. Struct. Biol. 16*, 644−653.

(3) Weil, J. A., and Bolton, J. R. (2007) *Electron Paramagnetic Resonance: Elementary Theory and Practical Applications*, Wiley-Interscience, Hoboken, NJ.

(4) Feher, G. (1956) Observation of Nuclear Magnetic Resonances via the Electron Spin Resonance Line. *Phys. Rev. 103*, 834−835.

(5) Mims, W. B. (1965) Pulsed Endor Experiments. *Proc. R. Soc. London, Ser. A 283*, 452−457.

(6) Davies, E. R. (1974) A new pulse endor technique. *Phys. Lett. A 47*, 1−2.

(7) Schweiger, A., and Jeschke, G. (2001) *Principles of Pulse Electron Paramagnetic Resonance*, Oxford University Press, New York.

(8) Rowan, L. G., Hahn, E. L., and Mims, W. B. (1965) Electron-Spin-Echo Envelope Modulation. *Phys. Rev. 137*, A61−A71.

(9) Mims, W. B. (1972) Envelope Modulation in Spin-Echo Experiments. *Phys. Rev. B 5*, 2409−2019.

(10) Dikanov, S. A., and Tsvetkov, Y. (1992) *Electron Spin Echo Envelope Modulation (ESEEM) Spectroscopy*, CRC Press, Boca Raton, FL.

(11) Höfer, P., Grupp, A., Nebenführ, H., and Mehring, M. (1986) Hyperfine sublevel correlation (HYSCORE) spectroscopy: A 2D ESR investigation of the squaric acid radical. *Chem. Phys. Lett. 132*, 279−282.

(12) Pannier, M., Veit, S., Godt, A., Jeschke, G., and Spiess, H. W. (2000) Dead-time free measurement of dipole-dipole interactions between electron spins. *J. Magn. Reson. 142*, 331−340.

(13) Jeschke, G., and Polyhach, Y. (2007) Distance measurements on spin-labelled biomacromolecules by pulsed electron paramagnetic resonance. *Phys. Chem. Chem. Phys. 9*, 1895−1910.

(14) Klare, J. P. (2012) Site-Directed Spin Labeling and Electron Paramagnetic Resonance (EPR) Spectroscopy: A Versatile Tool to Study Protein-Protein Interaction. In *Protein Interactions*, InTech, New York.

(15) Hubbell, W. L., Gross, A., Langen, R., and Lietzow, M. A. (1998) Recent advances in site-directed spin labeling of proteins. *Curr. Opin. Struct. Biol. 8*, 649−656.

(16) Berliner, L. J. (2010) From spin-labeled proteins to in vivo EPR applications. *Eur. Biophys. J. 39*, 579−588.

(17) Klug, C. S., and Feix, J. B. (2004) SDSL: A survey of biological applications. *Biol. Magn. Reson. 24*, 269−308.

(18) Drescher, M. (2012) EPR in protein science: Intrinsically disordered proteins. *Top. Curr. Chem. 321*, 91−119.

(19) Feix, J. B., and Klug, C. S. (2002) Site-Directed Spin Labeling of Membrane Proteins and Peptide-Membrane Interactions. In *Biological Magnetic Resonance*, pp 251−281, Springer, New York.

(20) Wuthrich, K. (2003) NMR studies of structure and function of biological macromolecules (Nobel Lecture). *J. Biomol. NMR 27*, 13−39.

(21) Acharya, K. R., and Lloyd, M. D. (2005) The advantages and limitations of protein crystal structures. *Trends Pharmacol. Sci. 26*, 10−14.

(22) Schiemann, O., and Prisner, T. F. (2007) Long-range distance determinations in biomacromolecules by EPR spectroscopy. *Q. Rev. Biophys. 40*, 1−53.

(23) Torres, J., Stevens, T. J., and Samso, M. (2003) Membrane proteins: The 'Wild West' of structural biology. *Trends Biochem. Sci. 28*, 137−144.

(24) Columbus, L., and Hubbell, W. L. (2002) A new spin on protein dynamics. *Trends Biochem. Sci. 27*, 288−295.

(25) Qin, P. Z., and Dieckmann, T. (2004) Application of NMR and EPR methods to the study of RNA. *Curr. Opin. Struct. Biol. 14*, 350−359.

(26) Speicher, D. W. (1998) Characterization of protein primary structure. *Dev. Biol. Stand. 96*, 27−28.

(27) Klare, J. P., and Steinhoff, H.-J. (2009) Spin labeling EPR. *Photosynth. Res. 102*, 377−390.

(28) Hubbell, W. L., McHaourab, H. S., Altenbach, C., and Lietzow, M. A. (1996) Watching proteins move using site-directed spin labeling. *Structure 4*, 779−783.

(29) Janez, S., Tilen, K., Zoran, A., Bogdan, F., David, S., and Hemminga, M. A. (2005) Spin Label EPR-Based Characterization of Biosystem Complexity. *J. Chem. Inf. Model. 45*, 394−406.

(30) Hustedt, E. J., and Beth, A. H. (1999) Nitroxide spin-spin interactions: Applications to protein structure and dynamics. *Annu. Rev. Biophys. Biomol. Struct. 28*, 129−153.

(31) Hustedt, E. J., Smirnov, A. I., Laub, C. F., Cobb, C. E., and Beth, A. H. (1997) Molecular distances from dipolar coupled spin-labels: The global analysis of multifrequency continuous wave electron paramagnetic resonance data. *Biophys. J. 72*, 1861−1877.

(32) Liu, K. J., Gast, P., Moussavi, M., Norby, S. W., Vahidi, N., Walczak, T., Wu, M., and Swartz, H. M. (1993) Lithium Phthalocyanine: A Probe for Electron-Paramagnetic-Resonance Oximetry in Viable Biological-Systems. *Proc. Natl. Acad. Sci. U.S.A. 90*, 5438−5442.

(33) Bordignon, E., and Steinhoff, H. J. (2007) Membrane protein structure and dynamics studied by site-directed spin-labeling ESR. *ESR Spectroscopy in Membrane Biophysics*, Vol. 27, pp 129−164, Springer, New York.

(34) Jeschke, G., Bender, A., Schweikardt, T., Panek, G., Decker, H., and Paulsen, H. (2005) Localization of the N-terminal domain in light-harvesting chlorophyll a/b protein by EPR measurements. *J. Biol. Chem. 280*, 18623−18630.

(35) Mchaourab, H. S., and Perozo, E. (2002) Determination of Protein Folds and Conformational Dynamics Using Spin-Labeling EPR Spectroscopy. In *Biological Magnetic Resonance* (Berliner, L., Eaton, G., and Eaton, S., Eds.) pp 185−247, Springer, New York.

(36) Perozo, E., Cortes, D. M., and Cuello, L. G. (1998) Three-dimensional architecture and gating mechanism of a K$^+$ channel studied by EPR spectroscopy. *Nat. Struct. Biol. 5*, 459−469.

(37) Vasquez, V., Sotomayor, M., Cortes, D. M., Roux, B., Schulten, K., and Perozo, E. (2008) Three-dimensional architecture of membrane-embedded MscS in the closed conformation. *J. Mol. Biol. 378*, 55−70.

(38) Stone, T. J., Buckman, T., Nordio, P. L., and McConnel, H. (1965) Spin-Labeled Biomolecules. *Proc. Natl. Acad. Sci. U.S.A. 54*, 1010−1017.

(39) Cornish, V. W., Benson, D. R., Altenbach, C. A., Hideg, K., Hubbell, W. L., and Schultz, P. G. (1994) Site-specific incorporation of biophysical probes into proteins. *Proc. Natl. Acad. Sci. U.S.A. 91*, 2910−2914.

(40) Steinhoff, H. J. (2004) Multi-frequency EPR spectroscopy studies of the structure and conformational changes of site-directed spin labelled membrane proteins. *Supramol. Struct. Funct. 8*, 157−177.

(41) Stoll, S., and Schweiger, A. (2007) Easyspin: Simulating cw ESR spectra. *Biol. Magn. Reson. 27*, 299−321.

(42) Columbus, L., Kalai, T., Jeko, J., Hideg, K., and Hubbell, W. L. (2001) Molecular motion of spin labeled side chains in α-helices: Analysis by variation of side chain structure. *Biochemistry 40*, 3828−3846.

(43) Lietzow, M. A., and Hubbell, W. L. (2004) Motion of spin label side chains in cellular retinol-binding protein: Correlation with structure and nearest-neighbor interactions in an antiparallel β-sheet. *Biochemistry 43*, 3137−3151.

(44) Cuello, L. G., Cortes, D. M., and Perozo, E. (2004) Molecular architecture of the KvAP voltage-dependent K$^+$ channel in a lipid bilayer. *Science 306*, 491−495.

(45) Budil, D. E., Lee, S., Saxena, S., and Freed, J. H. (1996) Nonlinear-Least-Squares Analysis of Slow-Motion EPR Spectra in One and Two Dimensions Using a Modified Levenberg−Marquardt Algorithm. *J. Magn. Reson., Ser. A 120*, 155−189.

(46) Feldmann, E. A., Ni, S., Sahu, I. D., Mishler, C. H., Risser, D. D., Murakami, J. L., Tom, S. K., McCarrick, R. M., Lorigan, G. A., Tolbert, B. S., Callahan, S. M., and Kennedy, M. A. (2011) Evidence for Direct Binding between HetR from *Anabaena* sp PCC 7120 and PatS-5. *Biochemistry 50*, 9212−9224.

(47) Mokdad, A., Herrick, D. Z., Kahn, A. K., Andrews, E., Kim, M., and Cafiso, D. S. (2012) Ligand-Induced Structural Changes in the *Escherichia coli* Ferric Citrate Transporter Reveal Modes for Regulating Protein-Protein Interactions. *J. Mol. Biol. 423*, 818−830.

(48) Ferguson, A. D., Chakraborty, R., Smith, B. S., Esser, L., van der Helm, D., and Deisenhofer, J. (2002) Structural basis of gating by the outer membrane transporter FecA. *Science 295*, 1715−1719.

(49) Ferguson, A. D., Amezcua, C. A., Halabi, N. M., Chelliah, Y., Rosen, M. K., Ranganathan, R., and Deisenhofer, J. (2007) Signal transduction pathway of TonB-dependent transporters. *Proc. Natl. Acad. Sci. U.S.A. 104*, 513−518.

(50) Humphrey, W., Dalke, A., and Schulten, K. (1996) VMD: Visual molecular dynamics. *J. Mol. Graphics 14*, 33−38.

(51) Hess, J. F., Budamagunta, M. S., Aziz, A., FitzGerald, P. G., and Voss, J. C. (2013) Electron paramagnetic resonance analysis of the vimentin tail domain reveals points of order in a largely disordered region and conformational adaptation upon filament assembly. *Protein Sci. 22*, 47−55.

(52) Aziz, A., Hess, J. F., Budamagunta, M. S., Voss, J. C., and FitzGerald, P. G. (2010) Site-directed Spin Labeling and Electron Paramagnetic Resonance Determination of Vimentin Head Domain Structure. *J. Biol. Chem. 285*, 15278−15285.

(53) Fajer, P. G. (2000) Electron Spin Resonance Labeling in Peptide and Protein Analysis. In *Encyclopedia of Analytical Chemistry* (Meyers, R. A., Ed.) pp 5725−5761, John Wiley & Sons, Ltd., New York.

(54) Altenbach, C., Greenhalgh, D. A., Khorana, H. G., and Hubbell, W. L. (1994) A Collision Gradient Method to Determine the Immersion Depth of Nitroxides in Lipid Bilayers: Application to Spin-Labeled Mutants of Bacteriorhodopsin. *Proc. Natl. Acad. Sci. U.S.A. 91*, 1667−1671.

(55) Dong, J. H., Yang, G. Y., and McHaourab, H. S. (2005) Structural basis of energy transduction in the transport cycle of MsbA. *Science 308*, 1023−1028.

(56) Malmberg, N. J., and Falke, J. J. (2005) Use of EPR power saturation to analyze the membrane-docking geometries of peripheral proteins: Applications to C2 domains. *Annu. Rev. Biophys. Biomol. Struct. 34*, 71−90.

(57) Yu, Y. G., Thorgeirsson, T. E., and Shin, Y. K. (1994) Topology of an amphiphilic mitochondrial signal sequence in the membrane-inserted state: A spin-labeling study. *Biochemistry 33*, 14221−14226.

(58) Klug, C. S., Su, W. Y., and Feix, J. B. (1997) Mapping of the residues involved in a proposed β-strand located in the ferric enterobactin receptor FepA using site-directed spin-labeling. *Biochemistry 36*, 13027−13033.

(59) Coey, A. T., Sahu, I. D., Gunasekera, T. S., Troxel, K. R., Hawn, J. M., Swartz, M. S., Wickenheiser, M. R., Reid, R.-j., Welch, R. C., Vanoye, C. G., Kang, C., Sanders, C. R., and Lorigan, G. A. (2011) Reconstitution of KCNE1 into Lipid Bilayers: Comparing the Structural, Dynamic, and Activity Differences in Micelle and Vesicle Environments. *Biochemistry 50*, 10851−10859.

(60) Kang, C., Tian, C., Sonnichsen, F. D., Smith, J. A., Meiler, J., George, A. L. J., Vanoye, C. G., Kim, H. J., and Sanders, C. R. (2008) Structure of KCNE1 and Implications for How It Modulates the KCNQ1 Potassium Channel. *Biochemistry 47*, 7999−8006.

(61) Voss, J., He, M. M., Hubbell, W. L., and Kaback, H. R. (1996) Site-directed spin labeling demonstrates that transmembrane domain XII in the lactose permease of *Escherichia coli* is an α-helix. *Biochemistry 35*, 12915−12918.

(62) Guan, L., Mirza, O., Verner, G., Iwata, S., and Kaback, H. R. (2007) Structural determination of wild-type lactose permease. *Proc. Natl. Acad. Sci. U.S.A. 104*, 15294−15298.

(63) Inbaraj, J. J., Cardon, T. B., Laryukhin, M., Grosser, S. M., and Lorigan, G. A. (2006) Determining the topology of integral membrane peptides using EPR spectroscopy. *J. Am. Chem. Soc. 128*, 9549−9554.

(64) Ghimire, H., Hustedt, E. J., Sahu, I. D., Inbaraj, J. J., McCarrick, R., Mayo, D. J., Benedikt, M. R., Lee, R. T., Grosser, S. M., and Lorigan, G. A. (2012) Distance Measurements on a Dual-Labeled TOAC AChR M2δ Peptide in Mechanically Aligned DMPC Bilayers via Dipolar Broadening CW-EPR Spectroscopy. *J. Phys. Chem. B 116*, 3866−3873.

(65) Liang, Z., and Freed, J. H. (1999) An Assessment of the Applicability of Multifrequency ESR to Study the Complex Dynamics of Biomolecules. *J. Phys. Chem. B 103*, 6384−6396.

(66) Zhang, Z. W., Fleissner, M. R., Tipikin, D. S., Liang, Z. C., Moscicki, J. K., Earle, K. A., Hubbell, W. L., and Freed, J. H. (2010) Multifrequency Electron Spin Resonance Study of the Dynamics of Spin Labeled T4 Lysozyme. *J. Phys. Chem. B 114*, 5503−5521.

(67) Earle, K. A., and Smirnov, A. I. (2004) High Field ESR: Applications to Protein Structure and Dynamics. In *Biological Magnetic Resonance*, pp 95−141, Kluwer Academic/Plenum Publishers, New York.

(68) Savitsky, A., and Mobius, K. (2009) High-field EPR. *Photosynth. Res. 102*, 311−333.

(69) Borbat, P. P., Costa-Filho, A. J., Earle, K. A., Moscicki, J. K., and Freed, J. H. (2001) Electron spin resonance in studies of membranes and proteins. *Science 291*, 266−269.

(70) Mobius, K., and Savitsky, A. (2008) *High-Field EPR Spectroscopy on Proteins and their Model Systems: Characterization of Transient Paramagnetic States*, Royal Society of Chemistry, London.

(71) Mobius, K., Savitsky, A., Schnegg, A., Plato, M., and Fuchs, M. (2005) High-field EPR spectroscopy applied to biological systems: Characterization of molecular switches for electron and ion transfer. *Phys. Chem. Chem. Phys. 7*, 19−42.

(72) Nesmelov, Y. E., Agafonov, R. V., Burr, A. R., Weber, R. T., and Thomas, D. D. (2008) Structure and dynamics of the force-generating domain of myosin probed by multifrequency electron paramagnetic resonance. *Biophys. J. 95*, 247−256.

(73) Bauer, C. B., Holden, H. M., Thoden, J. B., Smith, R., and Rayment, I. (2000) X-ray structures of the apo and MgATP-bound states of *Dictyostelium discoideum* myosin motor domain. *J. Biol. Chem. 275*, 38494−38499.

(74) Harrington, W. F., and Rodgers, M. E. (1984) Myosin. *Annu. Rev. Biochem. 53*, 35−73.

(75) McCracken, J. (2011) Electron Spin Echo Envelope Modulation (ESEEM) Spectroscopy. In *Encyclopedia of Inorganic and Bioinorganic Chemistry*, John Wiley & Sons, Ltd., New York.

(76) Cieslak, J. A., Focia, P. J., and Gross, A. (2010) Electron Spin-Echo Envelope Modulation (ESEEM) Reveals Water and Phosphate Interactions with the KcsA Potassium Channel. *Biochemistry 49*, 1486−1494.

(77) Zhou, A., Abu-Baker, S., Sahu, I. D., Liu, L., McCarrick, R. M., Dabney-Smith, C., and Lorigan, G. A. (2012) Determining α-Helical and β-Sheet Secondary Structures via Pulsed Electron Spin Resonance Spectroscopy. *Biochemistry 51*, 7417−7419.

(78) Volkov, A., Dockter, C., Polyhach, Y., Paulsen, H., and Jeschke, G. (2010) Site-Specific Information on Membrane Protein Folding by Electron Spin Echo Envelope Modulation Spectroscopy. *J. Phys. Chem. Lett. 1*, 663−667.

(79) Dzuba, S. A., and Raap, J. (2013) Spin-Echo Electron Paramagnetic Resonance (EPR) Spectroscopy of a Pore-Forming (Lipo)Peptaibol in Model and Bacterial Membranes. *Chem. Biodiversity 10*, 864−875.

(80) Sun, L., Hernandez-Guzman, J., and Warncke, K. (2009) OPTESIM, a versatile toolbox for numerical simulation of electron spin echo envelope modulation (ESEEM) that features hybrid optimization and statistical assessment of parameters. *J. Magn. Reson. 200*, 21−28.

(81) Liu, L., Sahu, I. D., Mayo, D. J., McCarrick, R. M., Troxel, K., Zhou, A., Shockley, E., and Lorigan, G. A. (2012) Enhancement of Electron Spin Echo Envelope Modulation Spectroscopic Methods to Investigate the Secondary Structure of Membrane Proteins. *J. Phys. Chem. B 116*, 11041−11045.

(82) Mayo, D., Zhou, A., Sahu, I., McCarrick, R., Walton, P., Ring, A., Troxel, K., Coey, A., Hawn, J., Emwas, A. H., and Lorigan, G. A. (2011) Probing the structure of membrane proteins with electron spin echo envelope modulation spectroscopy. *Protein Sci. 20*, 1100−1104.

(83) Chiang, Y.-W., Zheng, T.-Y., Kao, C.-J., and Horng, J.-C. (2009) Determination of Interspin Distance Distributions by cw-ESR Is a Single Linear Inverse Problem. *Biophys. J. 97*, 930−936.

(84) Kittell, A. W., Hustedt, E. J., and Hyde, J. S. (2012) Inter-spin distance determination using L-band (1−2 GHz) non-adiabatic rapid sweep electron paramagnetic resonance (NARS EPR). *J. Magn. Reson. 221*, 51−56.

(85) Rabenstein, M. D., and Shin, Y. K. (1995) Determination of the distance between 2 spin labels attached to a macromolecule. *Proc. Natl. Acad. Sci. U.S.A. 92*, 8239−8243.

(86) Altenbach, C., Oh, K. J., Trabanino, R. J., Hideg, K., and Hubbell, W. L. (2001) Estimation of inter-residue distances in spin labeled proteins at physiological temperatures: Experimental strategies and practical limitations. *Biochemistry 40*, 15471−15482.

(87) McHaourab, H. S., Oh, K. J., Fang, C. J., and Hubbell, W. L. (1997) Conformation of T4 lysozyme in solution. Hinge-bending motion and the substrate-induced conformational transition studied by site-directed spin labeling. *Biochemistry 36*, 307−316.

(88) Hanelt, I., Wunnicke, D., Muller-Trimbusch, M., Vor der Bruggen, M., Kraus, I., Bakker, E. P., and Steinhoff, H. J. (2010) Membrane Region M-2C2 in Subunit KtrB of the K⁺ Uptake System KtrAB from *Vibrio alginolyticus* Forms a Flexible Gate Controlling K⁺ Flux: An Electron Paramagnetic Resonance Study. *J. Biol. Chem. 285*, 28210−28219.

(89) Borbat, P. P., McHaourab, H. S., and Freed, J. H. (2002) Protein structure determination using long-distance constraints from double-quantum coherence ESR: Study of T4 lysozyme. *J. Am. Chem. Soc. 124*, 5304−5314.

(90) Schiemann, O., Piton, N., Mu, Y. G., Stock, G., Engels, J. W., and Prisner, T. F. (2004) A PELDOR-based nanometer distance ruler for oligonucleotides. *J. Am. Chem. Soc. 126*, 5722−5729.

(91) Milov, A. D., Tsvetkov, Y. D., Formaggio, F., Crisma, M., Toniolo, C., and Raap, J. (2000) Self-assembling properties of membrane-modifying peptides studied by PELDOR and CW-ESR spectroscopies. *J. Am. Chem. Soc. 122*, 3843−3848.

(92) Hilger, D., Jung, H., Padan, E., Wegener, C., Vogel, K. P., Steinhoff, H. J., and Jeschke, G. (2005) Assessing oligomerization of membrane proteins by four-pulse DEER: pH-dependent dimerization of NhaA Na⁺/H⁺ antiporter of *E. coli. Biophys. J. 89*, 1328−1338.

(93) Jeschke, G. (2012) DEER Distance Measurements on Proteins. *Annu. Rev. Phys. Chem.*, 419−446.

(94) Banham, J. E., Timmel, C. R., Abbott, R. J. M., Lea, S. M., and Jeschke, G. (2006) The characterization of weak protein-protein interactions: Evidence from DEER for the trimerization of a von Willebrand Factor A domain in solution. *Angew. Chem., Int. Ed. 45*, 1058−1061.

(95) Reginsson, G. W., Hunter, R. I., Cruickshank, P. A. S., Bolton, D. R., Sigurdsson, S. T., Smith, G. M., and Schiemann, O. (2012) W-band PELDOR with 1 kW microwave power: Molecular geometry, flexibility and exchange coupling. *J. Magn. Reson. 216*, 175−182.

(96) Prisner, T., Rohrer, M., and MacMillan, F. (2001) Pulsed EPR spectroscopy: Biological applications. *Annu. Rev. Phys. Chem. 52*, 279−313.

(97) McHaourab, H. S., Steed, P. R., and Kazmier, K. (2011) Toward the fourth dimension of membrane protein structure: Insight into dynamics from spin-labeling EPR spectroscopy. *Structure 19*, 1549−1561.

(98) Ghimire, H., McCarrick, R. M., Budil, D. E., and Lorigan, G. A. (2009) Significantly Improved Sensitivity of Q-Band PELDOR/DEER Experiments Relative to X-Band Is Observed in Measuring the Intercoil Distance of a Leucine Zipper Motif Peptide (GCN4-LZ). *Biochemistry 48*, 5782−5784.

(99) Polyhach, Y., Bordignon, E., Tschaggelar, R., Gandra, S., Godt, A., and Jeschke, G. (2012) High sensitivity and versatility of the DEER experiment on nitroxide radical pairs at Q-band frequencies. *Phys. Chem. Chem. Phys. 14*, 10762−10773.

(100) Zou, P., and McHaourab, H. S. (2010) Increased Sensitivity and Extended Range of Distance Measurements in Spin-Labeled Membrane Proteins: Q-Band Double Electron-Electron Resonance and Nanoscale Bilayers. *Biophys. J. 98*, L18−L20.

(101) Höfer, P., Heilig, R., and Schmalbein, D. (2003) The superQ-FT accessory for pulsed EPR, ENDOR and ELDOR at 34 GHz. *Bruker Spin Report*, pp 37−43, Bruker Corp.

(102) Fleissner, M. R., Bridges, M. D., Brooks, E. K., Cascio, D., Kálai, T., Hideg, K., and Hubbell, W. L. (2012) Structure and dynamics of a conformationally constrained nitroxide side chain and applications in EPR spectroscopy. *Proc. Natl. Acad. Sci. U.S.A. 108*, 16241−16246.

(103) Jao, C. C., Hegde, B. G., Chen, J., Haworth, I. S., and Langen, R. (2008) Structure of membrane-bound α-synuclein from site-directed spin labeling and computational refinement. *Proc. Natl. Acad. Sci. U.S.A. 105*, 19666−19671.

(104) Hirst, S. J., Alexander, N., McHaourab, H. S., and Meiler, J. (2011) RosettaEPR: An integrated tool for protein structure determination from sparse EPR data. *J. Struct. Biol. 173*, 506−514.

(105) Barrett, P. J., Song, Y., Van Horn, W. D., Hustedt, E. J., Schafer, J. M., Hadziselimovic, A., Beel, A. J., and Sanders, C. R. (2012) The Amyloid Precursor Protein Has a Flexible Transmembrane Domain and Binds Cholesterol. *Science 336*, 1168−1171.

(106) Dixit, M., Kim, S., Matthews, G. F., Erreger, K., Galli, A., Cobb, C. E., Hustedt, E. J., and Beth, A. H. (2013) Structural Arrangement of the Intracellular Ca²⁺ Binding Domains of the Cardiac Na⁺/Ca²⁺ Exchanger (NCX1.1) Effects of Ca²⁺ Binding. *J. Biol. Chem. 288*, 4194−4207.

(107) Hilger, D., Polyhach, Y., Jung, H., and Jeschke, G. (2009) Backbone Structure of Transmembrane Domain IX of the Na$^+$/Proline Transporter PutP of *Escherichia coli*. *Biophys. J. 96*, 217–225.

(108) Raba, M., Baumgartner, T., Hilger, D., Klempahn, K., Haertel, T., Jung, K., and Jung, H. (2008) Function of transmembrane domain IX in the Na$^+$/proline transporter PutP. *J. Mol. Biol. 382*, 884–893.

(109) Jung, H., Rubenhagen, R., Tebbe, S., Leifker, K., Tholema, N., Quick, M., and Schmid, R. (1998) Topology of the Na$^+$/Proline transporter of *Escherichia coli*. *J. Biol. Chem. 273*, 26400–26407.

(110) Wegener, C., Tebbe, S., Steinhoff, H. J., and Jung, H. R. (2000) Spin labeling analysis of structure and dynamics of the Na$^+$/proline transporter of *Escherichia coli*. *Biochemistry 39*, 4831–4837.

(111) Endeward, B., Butterwick, J. A., MacKinnon, R., and Prisner, T. F. (2009) Pulsed Electron-Electron Double-Resonance Determination of Spin-Label Distances and Orientations on the Tetrameric Potassium Ion Channel KcsA. *J. Am. Chem. Soc. 131*, 15246–15250.

(112) Reichmann, D., Rahat, O., Cohen, M., Neuvirth, H., and Schreiber, G. (2007) The molecular architecture of protein-protein binding sites. *Curr. Opin. Struct. Biol. 17*, 67–76.

(113) Sarewicz, M., Szytula, S., Dutka, M., Osyczka, A., and Froncisz, W. (2008) Estimation of binding parameters for the protein-protein interaction using a site-directed spin labeling and EPR spectroscopy. *Eur. Biophys. J. Biophys. Lett. 37*, 483–493.

(114) Kim, S., Brandon, S., Zhou, Z., Cobb, C. E., Edwards, S. J., Moth, C. W., Parry, C. S., Smith, J. A., Lybrand, T. P., Hustedt, E. J., and Beth, A. H. (2011) Determination of Structural Models of the Complex between the Cytoplasmic Domain of Erythrocyte Band 3 and Ankyrin-R Repeats 13–24. *J. Biol. Chem. 286*, 20746–20757.

(115) Braun, P., Naegele, B., Wittmann, V., and Drescher, M. (2011) Mechanism of Multivalent Carbohydrate-Protein Interactions Studied by EPR Spectroscopy. *Angew. Chem., Int. Ed. 50*, 8428–8431.

(116) Herget, M., Baldauf, C., Scholz, C., Parcej, D., Wiesmuller, K. H., Tampe, R., Abele, R., and Bordignon, E. (2011) Conformation of peptides bound to the transporter associated with antigen processing (TAP). *Proc. Natl. Acad. Sci. U.S.A. 108*, 1349–1354.

(117) James, Z. M., McCaffrey, J. E., Torgersen, K. D., Karim, C. B., and Thomas, D. D. (2012) Protein-Protein Interactions in Calcium Transport Regulation Probed by Saturation Transfer Electron Paramagnetic Resonance. *Biophys. J. 103*, 1370–1378.

(118) Stoll, S. (2011) *High-field EPR of bioorganic radicals*, Vol. 22, Royal Society of Chemistry, London.

(119) Stoll, S., Gunn, A., Brynda, M., Sughrue, W., Kohler, A. C., Ozarowski, A., Fisher, A. J., Lagarias, J. C., and Britt, R. D. (2009) Structure of the Biliverdin Radical Intermediate in Phycocyanobilin:-Ferredoxin Oxidoreductase Identified by High-Field EPR and DFT. *J. Am. Chem. Soc. 131*, 1986–1995.

(120) Tu, S.-L., Rockwell, N. C., Lagarias, J. C., and Fisher, A. J. (2007) Insight into the radical mechanism of phycocyanobilin-ferredoxin oxidoreductase (PcyA) revealed by X-ray crystallography and biochemical measurements. *Biochemistry 46*, 1484–1494.

(121) Tu, S. L., Gunn, A., Toney, M. D., Britt, R. D., and Lagarias, J. C. (2004) Biliverdin reduction by cyanobacterial phycocyanobilin:fer-redoxin oxidoreductase (PcyA) proceeds via linear tetrapyrrole radical intermediates. *J. Am. Chem. Soc. 126*, 8682–8693.

(122) Stubbe, J., and Cotruvo, J. A. (2011) *Ribonucleotide Reductase: Recent Advances*, Vol. 4, John Wiley & Sons, Ltd., New York.

(123) Barry, B. A., Chen, J., Keough, J., Jenson, D., Offenbacher, A., and Pagba, C. (2012) Proton-Coupled Electron Transfer and Redox-Active Tyrosines: Structure and Function of the Tyrosyl Radicals in Ribonucleotide Reductase and Photosystem II. *J. Phys. Chem. Lett. 3*, 543–554.

(124) Sjoberg, B. M., Reichard, P., Graslund, A., and Ehrenberg, A. (1977) Nature of Free-Radical in Ribonucleotide Reductase from *Escherichia coli*. *J. Biol. Chem. 252*, 536–541.

(125) Sjoberg, B. M., Reichard, P., Graslund, A., and Ehrenberg, A. (1978) Tyrosine Free-Radical in Ribonucleotide Reductase from *Escherichia coli*. *J. Biol. Chem. 253*, 6863–6865.

(126) Tomter, A. B., Zoppellaro, G., Schmitzberger, F., Andersen, N. H., Barra, A.-L., Engman, H., Nordlund, P., and Andersson, K. K.

(2011) HF-EPR, Raman, UV/VIS Light Spectroscopic, and DFT Studies of the Ribonucleotide Reductase R2 Tyrosyl Radical from Epstein-Barr Virus. *PLoS One 6*, e25022.

(127) Hogbom, M., Galander, M., Andersson, M., Kolberg, M., Hofbauer, W., Lassmann, G., Nordlund, P., and Lendzian, F. (2003) Displacement of the tyrosyl radical cofactor in ribonucleotide reductase obtained by single-crystal high-field EPR and 1.4-angstrom X-ray data. *Proc. Natl. Acad. Sci. U.S.A. 100*, 3209–3214.

(128) Gerfen, G. J., Bellew, B. F., Un, S., Bollinger, J. M., Stubbe, J., Griffin, R. G., and Singel, D. J. (1993) High-Frequency (139.5 Ghz) EPR Spectroscopy of the Tyrosyl Radical in *Escherichia coli* Ribonucleotide Reductase. *J. Am. Chem. Soc. 115*, 6420–6421.

(129) Lendzian, F. (2005) Structure and interactions of amino acid radicals in class I ribonucleotide reductase studied by ENDOR and high-field EPR spectroscopy. *Biochim. Biophys. Acta 1707*, 67–90.

(130) Crofts, A. R., Holland, J. T., Victoria, D., Kolling, D. R. J., Dikanov, S. A., Gilbreth, R., Lhee, S., Kuras, R., and Kuras, M. G. (2008) The Q-cycle reviewed: How well does a monomeric mechanism of the bc$_1$ complex account for the function of a dimeric complex? *Biochim. Biophys. Acta 1777*, 1001–1019.

(131) Styring, S., Sjoholm, J., and Mamedov, F. (2012) Two tyrosines that changed the world: Interfacing the oxidizing power of photochemistry to water splitting in photosystem II. *Biochim. Biophys. Acta 1817*, 76–87.

(132) McCarrick, M. R., and Britt, R. D. (2008) *Current Models and Mechanism of Water Splitting: Photosynthetic Protein Complexes*, Wiley-VCH Verlag GmbH & Co. KGaA, Berlin.

(133) Umena, Y., Kawakami, K., Shen, J.-R., and Kamiya, N. (2011) Crystal structure of oxygen-evolving photosystem II at a resolution of 1.9 Å. *Nature 473*, 55–60.

(134) Dismukes, G. C., and Siderer, Y. (1980) EPR Spectroscopic Observations of a Manganese Center Associated with Water Oxidation in Spinach Chloroplasts. *FEBS Lett. 121*, 78–80.

(135) Dismukes, G. C., and Siderer, Y. (1981) Intermediates of a Polynuclear Manganese center involved in Photosynthetic Oxidation of Water. *Proc. Natl. Acad. Sci. U.S.A. 78*, 274–278.

(136) Zimmermann, J. L., and Rutherford, A. W. (1986) Electron paramagnetic resonance properties of the S2 state of the oxygen-evolving complex of photosystem II. *Biochemistry 25*, 4609–4615.

(137) Zimmermann, J. L., and Rutherford, A. W. (1984) Electron-Paramagnetic-Resonance studies of the oxygen-evolving Enzyme of Photosystem-II. *Biochim. Biophys. Acta 767*, 160–167.

(138) Casey, J. L., and Sauer, K. (1984) Electron-Paramagnetic-Resonance detection of a Cryogenically Photogenerated Intermediate in Photosynthetic Oxygen Evolution. *Biochim. Biophys. Acta 767*, 21–28.

(139) Haddy, A., Lakshmi, K. V., Brudvig, G. W., and Frank, H. A. (2004) Q-band EPR of the S-2 state of Photosystem II confirms an S = 5/2 origin of the X-band g = 4.1 signal. *Biophys. J. 87*, 2885–2896.

(140) Kim, D. H., Britt, R. D., Klein, M. P., and Sauer, K. (1992) The Manganese Site of the Photosynthetic Oxygen-Evolving Complex Probed by EPR Spectroscopy of Oriented Photosystem-II Mem-branes: The g = 4 and g = 2 Multiline Signals. *Biochemistry 31*, 541–547.

(141) Pantazis, D. A., Ames, W., Cox, N., Lubitz, W., and Neese, F. (2012) Two Interconvertible Structures that Explain the Spectroscopic Properties of the Oxygen-Evolving Complex of Photosystem II in the S2 State. *Angew. Chem., Int. Ed. 51*, 9935–9940.

(142) Messinger, J., Nugent, J. H. A., and Evans, M. C. W. (1997) Detection of an EPR multiline signal for the S$_0$ state in photosystem II. *Biochemistry 36*, 11055–11060.

(143) Messinger, J., Robblee, J. H., Yu, W. O., Sauer, K., Yachandra, V. K., and Klein, M. P. (1997) The S$_0$ State of the Oxygen-Evolving Complex in Photosystem II Is Paramagnetic: Detection of an EPR Multiline Signal. *J. Am. Chem. Soc. 119*, 11349–11350.

(144) Dexheimer, S. L., and Klein, M. P. (1992) Detection of a Paramagnetic Intermediate in the S1-State of the Photosynthetic oxygen-evolving Complex. *J. Am. Chem. Soc. 114*, 2821–2826.

(145) Campbell, K. A., Peloquin, J. M., Pham, D. P., Debus, R. J., and Britt, R. D. (1998) Parallel polarization EPR detection of an S-1-state "multiline" EPR signal in photosystem II particles from *Synechocystis* sp. PCC 6803. *J. Am. Chem. Soc. 120*, 447−448.

(146) Peloquin, J. M., Campbell, K. A., Randall, D. W., Evanchik, M. A., Pecoraro, V. L., Armstrong, W. H., and Britt, R. D. (2000) Mn-55 ENDOR of the S-2-state multiline EPR signal of photosystem II: Implications on the structure of the tetranuclear Mn cluster. *J. Am. Chem. Soc. 122*, 10926−10942.

(147) Britt, R. D., Peloquin, J. M., and Campbell, K. A. (2000) Pulsed and parallel-polarization EPR characterization of the photosystem II oxygen-evolving complex. *Annu. Rev. Biophys. Biomol. Struct. 29*, 463−495.

(148) Hasegawa, K., Ono, T. A., Inoue, Y., and Kusunoki, M. (1999) Spin-exchange interactions in the S-2-state manganese tetramer in photosynthetic oxygen-evolving complex deduced from g = 2 multiline EPR signal. *Chem. Phys. Lett. 300*, 9−19.

(149) Zheng, M., and Dismukes, G. C. (1996) Orbital configuration of the valence electrons, ligand field symmetry, and manganese oxidation states of the photosynthetic water oxidizing complex: Analysis of the S-2 state multiline EPR signals. *Inorg. Chem. 35*, 3307−3319.

(150) Ahrling, K. A., and Pace, R. J. (1995) Simulation of the S-2 State Multiline Electron-Paramagnetic-Resonance signal of Photosystem-II: A Multifrequency Approach. *Biophys. J. 68*, 2081−2090.

(151) Zouni, A., Witt, H. T., Kern, J., Fromme, P., Krauss, N., Saenger, W., and Orth, P. (2001) Crystal structure of photosystem II from *Synechococcus elongatus* at 3.8 angstrom resolution. *Nature 409*, 739−743.

(152) Kulik, L. V., Epel, B., Lubitz, W., and Messinger, J. (2007) Electronic structure of the Mn$_4$OxCa cluster in the S-0 and S-2 states of the oxygen-evolving complex of photosystem II based on pulse Mn-55-ENDOR and EPR Spectroscopy. *J. Am. Chem. Soc. 129*, 13421−13435.

(153) Britt, R. D., Tang, X. S., Gilchrist, M. L., Lorigan, G. A., Larsen, B. S., and Diner, B. A. (1994) Histidine at the Catalytic Site of the Photosynthetic Oxygen-Evolving Complex. *Biochem. Soc. Trans. 22*, 343−347.

(154) Tang, X. S., Diner, B. A., Larsen, B. S., Gilchrist, M. L., Lorigan, G. A., and Britt, R. D. (1994) Identification of Histidine at the Catalytic Site of the Photosynthetic Oxygen-Evolving Complex. *Proc. Natl. Acad. Sci. U.S.A. 91*, 704−708.

(155) Yeagle, G. J., Gilchrist, M. L., McCarrick, R. M., and Britt, R. D. (2008) Multifrequency pulsed electron paramagnetic resonance study of the S-2 state of the photosystem II manganese cluster. *Inorg. Chem. 47*, 1803−1814.

(156) Yeagle, G. J., Gilchrist, M. L., Jr., Walker, L. M., Debus, R. J., and Britt, R. D. (2008) Multifrequency electron spin-echo envelope modulation studies of nitrogen ligation to the manganese cluster of photosystem II. *Philos. Trans. R. Soc., B 363*, 1157−1166.

(157) Stich, T. A., Yeagle, G. J., Service, R. J., Debus, R. J., and Britt, R. D. (2011) Ligation of D1-His332 and D1-Asp170 to the Manganese Cluster of Photosystem II from *Synechocystis* Assessed by Multifrequency Pulse EPR Spectroscopy. *Biochemistry 50*, 7390−7404.

(158) Stull, J. A., Stich, T. A., Service, R. J., Debus, R. J., Mandal, S. K., Armstrong, W. H., and Britt, R. D. (2010) C-13 ENDOR Reveals That the D1 Polypeptide C-Terminus Is Directly Bound to Mn in the Photosystem II Oxygen Evolving Complex. *J. Am. Chem. Soc. 132*, 446−447.

(159) Aznar, C. P., and Britt, R. D. (2002) Simulations of the H-1 electron spin echo-electron nuclear double resonance and H-2 electron spin echo envelope modulation spectra of exchangeable hydrogen nuclei coupled to the S-2-state photosystem II manganese cluster. *Philos. Trans. R. Soc., B 357*, 1359−1365.

(160) McConnell, I. L., Grigoryants, V. M., Scholes, C. P., Myers, W. K., Chen, P.-Y., Whittaker, J. W., and Brudvig, G. W. (2012) EPR-ENDOR Characterization of (O-17, H-1, H-2) Water in Manganese Catalase and Its Relevance to the Oxygen-Evolving Complex of Photosystem II. *J. Am. Chem. Soc. 134*, 1504−1512.

(161) Hoffman, B. M., Dean, D. R., and Seefeldt, L. C. (2009) Climbing Nitrogenase: Toward a Mechanism of Enzymatic Nitrogen Fixation. *Acc. Chem. Res. 42*, 609−619.

(162) Seefeldt, L. C., Hoffman, B. M., and Dean, D. R. (2012) Electron transfer in nitrogenase catalysis. *Curr. Opin. Chem. Biol. 16*, 19−25.

(163) Spatzal, T., Aksoyoglu, M., Zhang, L., Andrade, S. L. A., Schleicher, E., Weber, S., Rees, D. C., and Einsle, O. (2011) Evidence for Interstitial Carbon in Nitrogenase FeMo Cofactor. *Science 334*, 940−940.

(164) Orme-Johnson, W. H., Hamilton, W. D., Jones, T. L., Tso, M.-Y. W., Burris, R. H., Shah, V. K., and Brill, W. J. (1972) Electron-Paramagnetic Resonance of Nitrogenase and Nitrogenase Components from *Clostridium pasteurianum* W5 and *Azotobacter vinelandii* OP. *Proc. Natl. Acad. Sci. U.S.A. 69*, 3142−3145.

(165) Lee, H. I., Cameron, L. M., Hales, B. J., and Hoffman, B. M. (1997) CO binding to the FeMo cofactor of CO-inhibited nitrogenase: (CO)-C-13 and H-1 Q-band ENDOR investigation. *J. Am. Chem. Soc. 119*, 10121−10126.

(166) Pollock, R. C., Lee, H. I., Cameron, L. M., Derose, V. J., Hales, B. J., Ormejohnson, W. H., and Hoffman, B. M. (1995) Investigation of CO bound to inhibited forms of nitrogenase MoFe protein by C-13 ENDOR. *J. Am. Chem. Soc. 117*, 8686−8687.

(167) Lukoyanov, D., Dikanov, S. A., Yang, Z.-Y., Barney, B. M., Samoilova, R. I, Narasimhulu, K. V., Dean, D. R., Seefeldt, L. C., and Hoffman, B. M. (2011) ENDOR/HYSCORE Studies of the Common Intermediate Trapped during Nitrogenase Reduction of N$_2$H$_2$, CH$_3$N$_2$H, and N$_2$H$_4$ Support an Alternating Reaction Pathway for N-2 Reduction. *J. Am. Chem. Soc. 133*, 11655−11664.

(168) Crowder, M. W., Spencer, J., and Vila, A. J. (2006) Metallo-β-lactamases: Novel weaponry for antibiotic resistance in bacteria. *Acc. Chem. Res. 39*, 721−728.

(169) Griffin, D. H., Richmond, T. K., Sanchez, C., Moller, A. J., Breece, R. M., Tierney, D. L., Bennett, B., and Crowder, M. W. (2011) Structural and Kinetic Studies on Metallo-β-lactamase IMP-1. *Biochemistry 50*, 9125−9134.

(170) DeRose, V. J. (2009) *Characterization of nucleic acid-metal ion binding by spectroscopic techniques*, Royal Society of Chemistry, London.